N841－74－13

（配付限定）

高次化プルトニウム燃料の臨界実験計画（Ⅵ）

―領域炉心の臨界実験と解析

Program of TCA Critical Experiments for 3 W/o PuO_2-UO_2 Fuel Rods(Ⅵ)

Critical Experiments and Analysis on the Light Water Moderated PuO_2-UO_2 Lattices

１９７４年７月

動力炉・核燃料開発事業団

東　海　事　業　所

〒319-1184　茨城県那珂郡東海村大字村松4番地49
核燃料サイクル開発機構
技術展開部　技術協力課

T
TN841-74-13
(1974年6月7日)

高次化プルトニウム燃料の臨界実験計画 (VI)

—領域炉心の臨界実験と解析

実施責任者　青木　利昌（'74. 4～'74.5）
安久津英男（'73. 9～'74.3）
安孫子進朗（'72.10～'73.8）
宮脇　良夫（'72. 4～'72.9）

報　告　者　湯本　鎌三*　松浦祥次郎**
松本　忠邦*　小林　岩夫**
笹島　秀吉*　鶴田　晴通**
板川　和男*　大野　秋男**
梶山　登司*　須崎　武則**
村上　清信**

期　間：1972年4月1日 ～ 1974年5月31日

目　的：軽水炉用プルトニウム燃料（特に，高次化プルトニウムを使用した場合）の炉物理特性を測定し，あわせて燃料設計コードの検証を行なう。

要　旨：核分裂性プルトニウムの存在比が約75％である高次化プルトニウムを用いた3％富化混合酸化物燃料を使って，H／Puが295～922の範囲で，一連の臨界実験が行なわれ，臨界量，中性子束分布，出力分布，β_{eff}/ℓ等が測定された。PuO_2－UO_2燃料一領域炉心の材料バックリングBm^2はH／Puが530で最大となり，β_{eff}/ℓはUO_2系のそれの約½となった。また，高次化プルトニウム燃料に特徴的なこととして，^{241}Puのβ崩壊による反応度減少が1年間で約1ドルにも達すること，および自発中性子源レベルが高いので，反応度測定上に注意を要すること等が判明した。実験解析では，群定数コードとして，LASER－PNCおよび，UGMG42－THERMOSが使用され，2次元臨界計算コードとしてPDQ－5が使用された。計算値は測定値と良い一致を示し，燃料設計コードの精度の良さが検証された。本実験および解析は，原研との共同研究として実施されたものであり，さらに複雑な炉心体系についての実験と解析も進んでおり，幅広い実験データと計算手法の蓄積がなされている。本報告書は，JAERI－memo　5745と同一内容である。

＊　プルトニウム燃料部設計課
＊＊　原研動力試験炉部開発室

Abstract

A rapidly rising surplus of plutonium from light water reactors will be available for commercial recycle into the reactors in near future. Significant programes concerned with plutonium use have been conducted or planned by labolatories, industrial organizations and governments.

The experimental and analytical studies are beeing carried out in the Japan Atomic Energy Research Institute using the Japan Power Demonstration Reactor, and the light water critical assembly, TCA, in co-operation with the Power Reactor and Nuclear Fuel Development Corporation for gaining information on the characteristics of PuO_2-UO_2 fuel rods, assemblies and cores.

In this paper the experimental results and the evaluation on the calculational methods are reported on the PuO_2-UO_2 uniform lattices. The fuel utilized in this experiment is 3.0 wt % PuO_2-UO_2 of which density is 55 % T.D. Isotopic composition of ^{239}Pu, ^{240}Pu and ^{241}Pu are 68, 22 and 7 wt %. The experiments have been carried out on the lattices of five atomic ratios of H/Pu ----295, 402, 494, 704 and 922 ----, measuring critical core dimensions, reactivity effects of ^{241}Pu decay to ^{241}Am, neutron activation distributions by Au wires, power distributions by a gamma scanning method and β_{eff}/ℓ by a pulsed neutron method. In this study, the conventional codes LASER and UGMG42-THERMOS were used for the cell calculations and PDQ-5 was used for the two dimensional diffusion calculations.

Contents

1. Introduction

Recently, plutonium as a reactor fuel has become of general interest. A rapid surplus of plutonium from a light water reactor will be available for commercial recycle into the reactors in near future. The type of plutonium fuel for the thermal water reactor is focused on a mixture of plutonium and uranium dioxide (PuO_2-UO_2).

As a result of experimental and calculational studies of reactor physics, significant progress has been made in assessing the uncertainties in expected design method[1],[2]. The precision of the physics analysis in plutonium fueled cores relative to uranium fueled cores is needed to be more firmly established. The adequency of any calculational method that is used to design the reactor cores must be tested by applying the method to a variety of reactor experiments. For a satisfactory evaluation of the methods, the ranges of experiments for plutonium enrichment, H/Pu atom ratio, and plutonium composition are required to be greater than that needed for plutonium build up in uranium enriched reactors.

Uniform lattice experiments were carried out using a zero power critical facility (TCA) at the Japan Atomic Energy Research Institute. The objectives of this studies are to obtain the basic data of the nuclear characteristics loaded with mixed-oxide fuel of uranium and high burnup plutonium, and to evaluate the accuracy of the conventional reactor calculation for the mixed-oxide fueled system. The experiments include the measurements of critical mass, neutron flux and power distributions, and the ratio of delayed-neutron

fraction to prompt neutron life time. The isotopic composition of ^{239}Pu and ^{240}Pu were 68 and 22 wt%, respectively. The atom ratio of H/Pu in the lattice were varied in the range of 295 to 922.

In Section 2 of this paper, the description of experimental apparatus are given. The experimental results are presented in Section 3. The calculated results and their correlations with experimental ones are presented in Section 4. In the last section, conclusions are stated.

2. Experimental apparatus

2.1 general description of TCA

The critical assembly, TCA, is a light water moderated and controlled nuclear facility operating at low thermal and nuclear power levels to provide the means for obtaining experimental and nuclear research data, reactor design checkout, and engineering tests.

The TCA is comprised of the facility, assembly, systems, and components listed below;

a. TCA facility
b. Reactor assembly
c. Hydraulic system
d. Demineralizer system
e. Radiation monitoring system
f. Fuel handling and storage equipment
g. Waste disposal system
h. Neutron source and source handling equipment
i. Controls and instrumentation
j. Safety system

Each reactor core is built up in a 2.078 m in hight by 1.832 m in diam. cylindrical, open top, stainless steel tank. Grid plates are used to position but not to support fuel rods. The center-to-center spacing of the fuel elements may be changed by replacing the upper and lower grid plates, thus providing means of changing the lattice arrangement.

The reactor is controlled in normal operation by means of the moderator level in the core tank. The moderator level in the tank is determined by a manometer located in the reactor room with the read-out on the control console. It enables the height of the moderator to be determined to within approximately $\pm$0.1 mm.

The safety sheets provided as a component of the safety system are positioned between fuel rods and may be inserted into the reactor core in the event of a departure from normal operating conditions. These safety sheets have no effect on the data of the critical experiments.

2.2 Fuel rod specifications.

The fuel rod used in this experiments is composed of 3.0 wt% enriched PuO_2-UO_2 pellets and Zircaloy-2 cladding. A description of the fuel rod with the information on content and composition of the cladding tube and fuel components is given in Table 1 and Fig.1. The data when the fuel material was assayed is also shown. This assaying data is important because of ^{241}Pu decaying to ^{241}Am.

The PuO_2 powders were mixed with the natural UO_2 powders. The sizes of the PuO_2 particles are expected for the large part to be less than 40 μm. The PuO_2-UO_2 pellets were prepared by pre-sintering.

2.3 Lattice arrangements

Arrangements of the lattice in which the experiments were conducted are shown in Table 2. Each lattice was centered in the TCA tank. The fuel rods were positioned vertically with the grid plates at the upper and the lower endplug of the fuel rod as shown in Fig.2.

In all cases, the lattice is effectively fully reflected with light water in the horizontal direction. Above the active region of the lattice, there is no reflector, and the fuel pellets and the cladding tubes and/or the aluminum plugs are present. Under the active region of the lattice, the aluminum endplugs of the fuel rod and the aluminum structural material of the core tank are present. The thickness of the lower reflector is about 30 cm.

All the experiments were carried out with the lattices composed of square unit cells. The cross-sectional pattern of the array of the fuel rods was kept as square as possible, and an example of the pattern is shown in Fig.3.

3. Experiment

3.1 Multiplication characteristics

3.1.1 Critical size determination

The critical size is the most fundamental data for checking the nuclear calculation. Usually, in the critical size determination, fully reflected core dimensions are measured. However, in this experiment, the data of partially immersed rectangular prism cores were measured to simplify the comparison with the two dimensional diffusion calculations. The critical size of each lattice was determined by measuring the moderator water level and the number of fuel rods. The water level was limited under effective fuel height of 706 mm in this measurement. The precision

of the water level manometer was within ±0.1 mm, but the ambiguity in the absolute value was less than 0.5 mm of which reactivity worth was less than 0.01%ΔK/K. The temperature of the water was in the range 13~22°C and its reactivity worth was corrected to 20°C by the experimentally obtained moderator temperature coefficient as shown in Table 3. After all, the effective multiplication factor K_{eff} in this measurement was 1.0000 ±0.0001.

The fissile nuclide ^{241}Pu decays to ^{241}Am by a half life of 14.5 year[3]. The reactivity effect of the depletion of fissile ^{241}Pu and buildup of ^{241}Am has not been measured directly[4]. The reactivity decrease of the cores were obtained by measuring the critical water level increase in the time interval of about one year. The results are shown in Table 4. The effect was about 1 dollar in a year.

The relation between reactivity and water level were measured by the pulsed neutron technique that is written in section 3.4. Usually, it is more accurate to measure the small reactivity by the period technique than the pulsed neutron technique. The period technique was not available because the neutron source level was too high to measure the reactor period at the usual power level of the TCA as written below. And it should be noticed also that the period-reactivity relation depends slightly on the ratio of atomic number density of H to Pu as shown in Table 5.

The neutron emission from the spontaneous fission of plutonium and the $^{18}O(\alpha,n)^{21}Ne$ reaction disturbs to determine the accurate critical states in low power level and also to use the period technique. The amount of neutrons from the PuO_2-UO_2 fuel is estimated and listed in Table 6. Neutrons from a fuel rod are 4.1×10^{3}n/sec. Total neutrons from 590 fuel rods are 2.4×10^{6}n/sec.

This will be multiplied to the value equivalent to the amount of fission neutron by chain reaction at the power level of about a few Watt when the multiplication factor K_{eff} of the core is 0.99999, ~-0.2 cent of subcriticality. The all critical conditions were then measured at the power level higher than 5 watt to estimate the critical condition by the ambiguity of less than 0.1 cent.

In case of the lattice of which water to fuel volume ratio was 1.77, the available number of the 3.0 wt % PuO_2-UO_2 fuel rods was insufficient to make the lattice critical. Other types of fuel rods which were 3.4 wt % PuO_2-UO_2 and 2.6 wt % UO_2 fuel rods were loaded additionally to atain criticality. The specifications of those additional fuel rods are shown in Table 7 and Figs.4 and 5.

Two geometrical configurations of the lattices were assembled and their cross-sectional patterns were cylindrical and square as shown in Figs.6 and 7. The additional fuel rods were loaded at periphery of the lattices. The criticality data, the number of fuel rods, water level, and temperature, are shown in Table 8. The square cross-sectional core needed more fuel rods than that of cylindrical.

Critical mass of the cylindrical core composed of the 3.0 wt % PuO_2-UO_2 fuel rods was estimated from the reactivity difference between the 3.4 wt % PuO_2-UO_2 and the 3.0 wt % PuO_2-UO_2 fuel rods. The reactivity of a fuel rod at the periphery of the cylindrical core was 6.4 cent for 3.4 wt % PuO_2-UO_2 and 3.4 cent for 3.0 wt % PuO_2-UO_2 fuel. Thus, the reactivity of the core composed of 3.0 wt % PuO_2-UO_2 fuel rods was estimated as -148 ± 12 cent at water level of 687.9 mm and at temperature of 21.3°C. This reactivity was converted to the effective multiplication factor of 0.9943 ± 0.0007

by using the calculated effective delayed neutron fraction, β_{eff}, of 0.00385.

3.1.2 Reflector savings

Reflector savings are one of the important quantities of reactor properties. In the few group constants calculations, geometrical bucklings are used to calculate neutron spectrum. In the two dimensional diffusion calculations, vertical bucklings are used to estimate neutron leakage from the core. The ambiguity in the vertical bucklings especially becomes a source of large error in the calculated multiplication factor. These bucklings were obtained from the critical core dimensions and reflector savings.

The reflector savings were determined by the epi-Cd Au activation distributions and the power distributions shown in Section 3.2 and 3.3. These distributions were fitted by the least equares technique to the cosine functions in two directions represented in Fig.8 except the data of core-reflector boundary as

$$y = A \cos (Bx + C), \qquad (1)$$

for the direction of each coordinate axis,

$$Y = A \cos^2(Bx + C) \qquad (2)$$

for diagonal direction, then

$$\lambda_H = \frac{\pi}{B} - W, \qquad (3)$$

$$\lambda_V = \frac{\pi}{B} - L, \qquad (4)$$

where A,B,C : constants,

λ_H : horizontal reflector saving consisting of both sides of core,

λ_V : vertical reflector saving consisting of upper and bottom sides of core,

W : effective core width,

L : effective core height.

The activation distributions of epi-Cd Au wires are used to obtain the reflector savings because the distributions are smooth and have no ripple as shown in the activity distributions by bare Au wire. Essentially, both distributions are same over the internal part of core. The fact is shown in Fig.23 as that the Cd-Ratio - 1.0, (R_{Cd}-1.0), of Au activity is constant in the core region. The obtained horizontal and vertical reflector savings are shown in Table 9 and Figs.9 and 10. The relation between the reflector savings and the water to fuel volume ratio were empirically determined by least square fittings, and the following formulae were obtained,

$$\lambda_H = \frac{6.285}{VR - 0.1048} + 11.92 \qquad (5)$$

$$\lambda_V = \frac{2.583}{VR - 0.9347} + 10.77 \qquad (6)$$

The calculated horizontal reflector savings are also shown in Fig.9. Experimental results show that the horizontal reflector savings decrease from 15.7 to 13.1 cm and the vertical savings also from 13.9 to 11.3 cm as the water to fuel volume ratio increase.

3.1.3 Critical masses and material bucklings

In the rectangular prism core, the minimum critical condition will be determined on a cubical core configurations, then the next relation holds,

$$f(X,Y,Z) \equiv \frac{\{(X+\lambda_H)(Y+\lambda_H)\}^{1/2}}{(Z+\lambda_V)} = 1 , \qquad (7)$$

where X,Y,Z are core dimensions. The minimum critical mass was obtained from the measured several sets of critical sizes by

fitting the critical masses to the quadratic curve as a function of $f(X,Y,Z)$ as shown in Fig.11. The extraporated minimum critical masses are shown in Table 10 with the ratio of atomic number density of H to Pu in the lattices. The material bucklings are obtained from the critical data in Table 4 and the reflector savings in Table9. The indicated experimental errors in the bucklings are standard deviations in different core patterns of the same water to fuel volume ratio. The minimum critical masses and the material bucklings are shown in Fig.12 with the ratio H/Pu. The maximum value of the material bucklings and the minimum value of the critical masses are observed at about 530 and 670 of H/Pu.

3.2 Activation distributions by Au wires

The transverse neutron density distributions in the lattices were measured by the activation of Au wires. Two Au wires of 0.4 mmϕ were stretched through the lattice between both sides of reflector in the x-y direction. One of the wires was covered by a 0.5mm thick Cd tube. After the irradiation the wires were unloaded from the lattices and cut into segments of which length was 1/2 of the lattice pitch at the core region and was 1/4 near the core boundary. The integral γ-ray above 0.3 MeV were measured by a well-type NaI(Tl) scintillation counter including a photo peak of 0.412 MeV of ^{198}Au. The segments were weighed twice by a balance of which sensitivity was 0.01 mg. The weights were used to correct the relative sensitivity of the segments. The experimental error was less than $\pm$ 1 % for the relative activities of the Au segments and less than $\pm$ 1 mm for identifing their positions. The results are shown in Fig.13 through 17 for the sub-Cd activities, in Figs.18 through 22 for the epi-Cd activities, in Fig.23 for

the activity ratio of sub-Cd to epi-Cd, R_{Cd}-1.0, and in Fig.48 the relation between R_{Cd}-1.0 and H/Pu. The digital values of them are shown in Appendix 1.

The sub-Cd activity shows fine structure in a fuel cell, increasing on cell boundary and decreasing beside a fuel rod. When the cutting of the wires were done precisely this feature appears clearly as shown in Fig.17.

3.3 Power distributions

The horizontal and vertical power distributions in the lattices were obtained measuring the fission product γ-rays from the irradiated fuel rods. Fission product γ-rays above 0.6 MeV were measured by a NaI(Tl) scintillation counter as shown in Fig.24. The time-dependent decay of the fission product γ-rays was corrected by a scheme previously measured by another experiment[5]. The experimental error was estimated by less than ±1.5%. The statistical error of γ-rays counting was less than ±1.0% and the error in the correction for the γ-ray time decay was less than ±1.0%. The results of horizontal power distributions are shown in Figs. 25 through 33 with the calculated values. The measured directions in the cores are represented in the figures where the results are shown. The average value in the x-y direction was normalized to unity. The vertical power distributions are shown in Figs.34 and 35. The vertical reflector savings were obtained from these distributions.

3.4 β_{eff}/ℓ and water level worth by pulsed-neutron technique

β_{eff}/ℓ

The ratio of effective delayed-neutron fraction to prompt neutron lifetime β_{eff}/ℓ has been deduced from the measurement by the pulsed-neutron technique[6] in rectangular loadings except

the core of which water to fuel volume ratio 1.77. The lattices used for the measurements are shown in Table 11 and Fig.36.

The nuclear reaction of pulsed source was of the (D,T) type and the source strength was about 10^6 neutrons per burst. The neutron was detected by using a uranium fission counter which was located at the core-reflector boundary, and the time profile of neutron density was recorded with a 256 channel analyzer. Approximately a half of the channels was used to observe the prompt neutron decay with the remaining half for the background. A schematic of the experimental equipments is given in Fig.37.

In the measurement three kinds of problems as follows were considered.

(1) Resolving time of the detector and associated circuitry.
Because of the low count rates and relatively short resolving time of 5 μs, it was not necessary to take into account resolving time of the system. Maximum count rate in this experimental series was a few pulses per one channel a sweep.

(2) Background
There were two sources of background in these measurement; The usual steady-state room background observed with any counter, and the background arising from delayed neutron production. Since the process of interest was the decay of the prompt neutrons only, the sum of these two backgrounds must be subtracted from the data.

(3) Harmonics
Since the pulsed neutron source was located near a face of the assembly, the distribution of thermal neutron following a burst was a superposition of many harmonics. The fundamental mode was eventually detectable because the higher

harmonics decayed rapidly to negligible proportions. In addition, some time must elapsed before the source neutrons were sufficiently thermalized to cause fissions. The combinations of these two effects---special harmonics and slowing-down of source neutrons ---produced a deviation from the purely exponential decay of the fundamental. These effects were eliminated in practice by observing the relation of a prompt neutron decay constant α with fitting ranges of the data to an exponential form

$$Y(t) = A \cdot \exp(-\alpha \cdot t) + B, \qquad (8)$$

where A and B are constants.

The reactivity ρ by the pulsed-neutron technique is obtained as

$$\rho = (1 - \frac{\alpha_H}{\alpha_C}) \beta_{eff} \qquad (9)$$

where α_H and α_C are prompt neutron decay constant at water level H and at critical water level, and β_{eff} is effective delayed neutron fraction. Otherhands, ρ is expressed by the one point model as

$$\rho = 1 - \frac{1 + M^2 B_r^2}{K_\infty} - \frac{M^2}{K_\infty} B_z^2 \qquad (10)$$

where M^2, K_∞, B_r^2, and B_z^2 are migration area, infinite multiplication factor, radial buckling, and vertical buckling respectively. From Eqs.(9) and (10), the linear relation between B_z^2 and α_H is obtained as

$$\alpha_H = a \cdot B_z^2 (H) + b \qquad (11)$$

where a and b are constants and $B_z^2(H)$ is an vertical buckling at a water level H. To obtain B_z^2 (H), the reflector saving in the vertical direction written in Section 3.1.2 was used. The decay constants of the fundamental mode at the critical, α_c, was determined by extraporating the equation to the critical water level. At delayed critical state the relation $\alpha_c = \beta_{eff}/\ell$ exists. An

example of the relation between α and $B_z^2(H)$ is shown in Fig.38 for the core of which water to fuel volume ratio is 2.98. The obtained α_c of each core is shown in Table 12 and Fig.39.

β_{eff}/ℓ of UO_2 lattices

To compare with UO_2 lattices, α_c was measured also about several lattices consisted of 2.6 wt % enriched UO_2 fuel rods. Specifications of the fuel rod are shown in Table 7 and Fig.4. The lattices used are shown in Table 13 and Fig.40. Measured and calculated results are shown in Table 14. In Fig. 41 and 42, the comparisons between PuO_2-UO_2 lattices for β_{eff} and β_{eff}/ℓ are shown. These show β_{eff} of PuO_2-UO_2 lattices are about 1/2 of that of UO_2 lattices. The β_{eff} is almost independent of the water to fuel volume ratio, on the contrary β_{eff}/ℓ depends greatly on it. It means neutron genelation time increases greatly with the ratio.

Water level reactivity worth and M^2/K_∞

The reactivity worth of the water level is in the unit of dollar obtained from

$$\Delta\rho_{H_0 \to H_1} = \frac{1}{\beta_{eff}} \cdot \frac{M^2}{K_\infty} \left(B_{z,H_0}^2 - B_{z,H_1}^2 \right), \qquad (12)$$

where

$$\frac{1}{\beta_{eff}} \cdot \frac{M^2}{K_\infty} = \frac{a}{\alpha_c} \qquad (13)$$

The relation a/α_c vs. H/Pu is shown in Table 15 and Fig.43. The relation was fitted to a linear function and represented as

$$a/\alpha_c = 1.74R + 7.25 \times 10^3 \qquad (14)$$

Where R is the ratio of the atomic number density of H to Pu. This linear relation had a error of $\pm$ 3.3 % over the measured range of H/Pu.

The ratio of migration area to infinite multiplication factor, M^2/K_∞, was obtained from the eq. (13) using calculated β_{eff} presented at Table 12 and is shown in Table 16 and Fig.44.

3.5 Discussions

Reactivity effects by manufacturing tolerances are mainly depend on fuel grid plate fabrication accuracy and the fuel rod diameter. For the other data, such as fuel pellet density and fuel stack weight, the inspected average values were used. The accuracy of the distance between the core center and any hole for a fuel rod is less than $\pm$ 0.05 mm. The reactivity change due to the slightly change of core dimensions is estimated using eq.(12). If the core was enlarged by 0.1 mm in x-y direction, the reactivity would be increased by about 3×10^{-5} ΔK/K, and was negligible small. The fabrication data of fuel rod diameter was 12.21 mm. However, in the calculation the value 12.23 mm has been used according to the design specification. The reactivity worth due to the difference of - 0.02 mm was estimated using the infinite multiplication factor and reactivity relation. The reactivity effect was less than 2×10^{-4} ΔK/K for the all lattices. The experimental results are not corrected by this effect.

It should be noticed that, in this experiment, the pre-sintered low density PuO_2-UO_2 pellet is used of which density is 6.056 g/cm^3, 55.21% T.D. If the considerable differences or uncertainties exist on the reactor physical characteristics in the utilization of the pellet instead of the usual sintered pellet, this experimental results will not be used for the check out of the usual calculational method. Some calculational surveys had been carried out about the 3.4 wt % PuO_2-UO_2 shown in Table 7. In the calculation made by LASER, some changes were observed about K_{∞}, B_m^2, M^2, τ_{fast}, $\eta_{thermal}$, P_{28}, etc., however, the differences of few group constants between pre-sintered and sintered pellets had not considerable dependence on the ratio of atomic number

density of H to Pu. As the results, the neutron slowing down, the resonance capture of fast neutron and the thermal neutron absorption would be affected slightly by the densification of the pre-sintered pellet increasing atomic number density of natural uranium. However, the effects would not change the characteristics which exist between the reactor physical properties and the ratio of H/Pu.

4. Correlations of calculation with experimental results

4.1 Calculational method

The procedures of calculations about the lattices are shown in Fig.45. The codes LASER[8] and UGMG42 - THERMOS[9].[10] were utilized in spectrum calculations and few group constants were obtained for the subsequent use in the diffusion calculations. The originals of the both methods are the MUFT code in fast section and THERMOS in thermal section. The calculational conditions are shown in Tables 17 and 18. The differences in the calculational methods of the both codes lie mainly on the cross section library, the thermal cut-off energy, the energy mesh structure, and the calculational method of resonance escape probability. The library of UGMG42-THERMOS based on the set evaluated by the Japan Nuclear Data Committee, and in LASER a modified library which contains the original LASER library and five nuclides, ^{237}Np, ^{239}Np, ^{238}Pu, ^{241}Am, ^{243}Am was used. The energy meshes in LASER are finer around the resonance peaks of ^{239}Pu and ^{240}Pu than those in UGMG42-THERMOS. Since the ^{241}Pu decays to ^{241}Am at the half life of 14.5 year, the calculated results were compared with the experimental results at the date, May16, 1972,....330 days after purification of plutonium. Atomic number densities at the date are shown in Table 19. The energy

ranges of broad groups are shown in Table 20. Three group constants obtained by LASER and UGMG42-THERMOS codes for the diffusion calculations and four group constants obtained by the UGMG42-THERMOS codes for the kinetic parameter calculations are shown in Table 21, 22, and 23.

Two dimensional diffusion calculations were performed with PDQ-5[11] and KAK[12] codes. An example of the plan view of spatial mesh points and edit regions are shown in Fig.46. The thickness of the reflector region was assumed to be 30 cm in all cores. The measured vertical reflector savings were used with the critical core height in the vertical neutron leakage calculation. The effective multiplication factor, the neutron flux distribution and the power distribution were calculated by the PDQ-5 using the three group constants. The effective delayed-neutron fraction β_{eff} and prompt-neutron life time were calculated by the two dimensional perturbation code KR302DPT[13] with the neutron flux and adjoint neutron flux obtained by the KAK in four neutron energy groups.

4.2 Multiplication factors

The calculations were carried out using the atomic number densities of 330 days after purification of plutonium shown in Table 19. The temperature and the vertical reflector saving of the lattices were supposed to be 20°C and 12.0 cm. Three kinds of corrections written below were made for the measured multiplication factors, K_{eff}, to compare with the calculated results and are shown in Table 24.

a) The temperature of the core changed in this measurement from 13 to 21°C. The reactivity differences from the 20°C were corrected by the measured temperature-reactivity relation shown in Table 3.

b) The reactivity difference due to ^{241}Pu decay to ^{241}Am in the

interval between the measured and calculated time were corrected by the measured results shown in Table 4.

c) The vertical reflector saving in each lattice was measured and are shown in Table 9. The reactivity differences due to the descrepancies between calculated and measured vertical reflector savings were corrected by the water level-reactivity relation measured by the pulsed neutron technique written in Section 3.4.

The multiplication factors obtained from the two dimensional diffusion calculations are shown in Table 25 with the core configurations and lattice parameters. The comparisons with the measured values are also made in the table. The differences of K_{eff} using LASER increase with water to fuel volume ratio or the ratio of atomic number density of H to Pu from -0.24 to 0.70 % ΔK/K, while that of UGMG42-THERMOS decrease from 2.14 to 0.28 % ΔK/K as shown in Fig.47.

4.3 Neutron flux distributions

Thermal neutron density distribution

The cross-section of Au in thermal neutron energy has the 1/v characteristics. The measured sub-Cd Au activity shows the neutron number density distributions. The distributions show fine structure in the lattices, increasing at cell boundary and decreasing beside fuel rods. The calculated thermal neutron density N was obtained as

$$N = \phi \cdot d \cdot \frac{1}{v_b} \qquad (15)$$

where ϕ : thermal neutron flux obtained by the two dimensional diffusion calculation,

d : thermal neutron flux depression factor, ϕ_b/ϕ_{av}

ϕ_b : thermal neutron flux at cell boundary of a unit cell in the spectrum calculation,

ϕ_{av}: average thermal neutron flux in a unit cell in the spectrum calculation, and

v_b : average thermal neutron velocity at cell boundary of an unit cell in the spectrum calculation.

The calculated v_b and d are shown in Table 26.

The spectrum calculations in an unit cell were performed for the cylindrical geometry, while the shape of the fuel cells were square. The differences on the average velocity due to the geometrical difference were neglected.

The calculated neutron density distributions are compared with the experimental results normalized to unity in the core region and are shown in Fig.13 through 17. The agreements between the calculated distributions by the both methods are good and the differences of them are less than 3% that will be due to the differences of the neutron energy ranges in the calculations. The root mean square differences between the experimental and calculated values range from 2 to 4 % in the core region. This difference is mainly due to the fact that the thermal neutron distributions in the lattices have ripple corresponding to the lattice pitches, and will be decreased when the difference is evaluated between the average values at each fuel cell and the calculated results. In the reflector region, the calculation underestimated the experimental thermal neutron density by about 3 to 5 % for all lattices.

Epi-thermal neutron flux distributions

The calculated epi-thermal neutron flux distributions in the lattices were compared with the epi-Cd neutron activation distributions of Au wires and are shown in Figs.18 through 22.

The calculational and experimental values are also normalized to unity in the core region.

The agreements between the calculated distributions by the both methods are better than that of thermal neutron density distributions. The differences between the both methods are slightly observed also as on the thermal neutron density distributions that would depend on the neutron energy ranges in the calculations. The distributions calculated by using LASER are slightly higher in the middle of the core region and lower in the outer side of the core region than that of using UGMG42-THERMOS.

The calculated results agree with the experimental values in less than 2.5 % at core region, but the difference of them in reflector region are 3 to 12 %. The difference decreases from 12 to 3 % with the water to fuel volume ratio. This difference would be due to the neutron energy dependence of Au absorption cross-section. The activity distributions of Au wires indicates the reaction rates with the more thermalized neutron flux than the calculated epi-thermal neutron flux. The calculated neutron fluxes are of the energy ranges of 0.625 eV~5.53 KeV and 1.855 eV~5.53 KeV, and are not able to be compared with the experimental activities in fact, because Au activities are mainly depend on the resonance absorption at 4.9 eV. However, they are approximately compared with each other since it is usually applyed that the relative epi-thermal neutron flux distributions in the core do not so depend on the neutron energy.

Cadmiun ratio

In an infinite uniform medium, the cross-section ratio of the epi-thermal slowing down to the thermal absorption, $\Sigma_{r,2}/\Sigma_{a,3}$, is related to the ratio of the thermal to the epi-thermal neutron fluxes by the simple diffusion theory as

$$\Sigma_{r,2}/\Sigma_{a,3} = \phi_3/\phi_2 \qquad (16)$$

In the present experimental core, D_3B^2 are much less than $\Sigma_{a,3}$, then the above relation approximately holds. Since the Au activity ratio of sub-Cd to epi-Cd has a relation to the ratio, ϕ_3/ϕ_2 ,

$$R_{Cd} - 1.0 = \Sigma_{r,2}/\Sigma_{a,3} \qquad (17)$$

These experimental and calculational results are shown in Figs. 23, 48,49 and in Table 27. The linear relation of R_{Cd}-1.0 or $\Sigma_{r,2}/\Sigma_{a,3}$ with H/Pu are observed in Fig. 48 and those between R_{Cd} - 1.0 and $\Sigma_{r,2}/\Sigma_{a,3}$ in Fig. 49.

4.4 Power distributions

The power distributions calculated by the two dimensional diffusion theory using two kinds of the cross-section sets are compared with each other and with the experimental results. The pointwise power at each mesh and the average power in each fuel cell are compared in Figs. 25 through 33 with the experimental results. They are normalized to the average power on the x-y direction represented in the figures for each core.

The differences between the calculated distributions by two methods are as small as that of the thermal neutron density and epi-thermal neutron flux distributions. The root mean square difference of the calculated powers to the experimental are shown

in Table 28. The maximum discrepancies are observed near the core-reflector boundary, and the differences are less than 5 % The differences are greater on the diagonal positions than the x-y positions in the cores. The calculations by using LASER agrees slightly better with the experiment than that by UGMG42-THERMOS.

4.5 Reactivity effect due to ^{241}Pu decay to ^{241}Am

The nuclide ^{241}Pu decays with a half-life of about 14.5 years accumulating ^{241}Am. The reactivity decrease due to the fact was calculated for the cores shown in Table 21 by the PDQ-5 code using three group cross-section sets by LASER in which the cross-sections of ^{241}Am were accounted as shown in Table 18 and Fig. 50. The experiments were carried out in the time interval of about one year as shown in Table 4. The reactivity changes were calculated for the time interval of 220 days, between May 16, 1972, 330 days after purification of plutonium and December 22, 1973, 550 days after the purification. The plutonium composition in the interval changed as shown in Table 29. The ^{241}Pu depleted from 7.01 to 6.81 wt % and the ^{241}Am built up from 0.308 to 0.506 wt %. The three group constants calculated by LASER using the data of Devember 22, 1972, 220 days after the initial calculations are shown in Table 30. In the interval of 220 days the thermal absorption cross-section $\Sigma_{a,3}$ decreased only about 0.08 % but the thermal fission cross-section $\Sigma_{f,3}$ decreased about 0.3 % for every lattice.

The calculated results by PDQ-5 are shown in Table 31 with experimental results. The reactivity changes of about 0.27 cent per day were obtained supporsing the linearity of the ^{241}Pu depletion in the interval. The calculational results agreed with the experimenta

results within the experimental error except one lattice.

4.6 Reflector savings

In the two dimensional diffusion calculations, a radial buckling, B_r^2, is represented independently on neutron energy group as

$$(B_r^2 D_g + \Sigma_g^t)\phi_g = \frac{\chi_g}{\lambda}\sum_{j=1}^{G} \nu\Sigma_j^f \phi_j + \Sigma_{g-1}^r \phi_{g-1} \quad , \qquad (18)$$

where $\Sigma_g^t = \Sigma_g^a + \Sigma_g^r + D_g B_g^2$: total cross-section,

Σ^a : absorption,

Σ^r : removal

g : suffix of neutron energy group,

D : diffusion coefficient,

B_g^2 : vertical buckling,

χ : fission neutron spectra, and

λ : eigen value.

The horizontal reflector saving was calculated from the B_r^2 by the following relation

$$B_r^2 = B_x^2 + B_y^2 = \left(\frac{\pi}{W + \lambda_H}\right)^2 + \left(\frac{\pi}{L + \lambda_H}\right)^2 \qquad (19)$$

for every core, where W and L were core dimensions in x and y directions and λ_H was horizontal reflector saving having the same meaning written in Section 3.1.2. The results are shown in Table 32 and Fig.9 with the experimental results. The calculated horizontal reflector savings by the both calculational methods, UGMG42-THERMOS and LASER, have the almost similar tendency with the experimental values depending on the water to fuel volume ratios of the lattices. The calculated results by using UGMG42-THERMOS overestimates the experimental values by about 3∼8 % while that of LASER agrees in the range of the experimental errors. This qualitative features are observed in the neutron

flux or the power distributions as that the calculated distributions by using UGMG42-TERMOS have slightly gentle form than that of LASER.

4.7 Effective delayed-neutron fraction and prompt-neutron life-time

Effective delayed-neutron fraction β_{eff} and prompt-neutron life-time ℓ were calculated by the two dimensional perturbation code KR302DPT[13] with the neutron flux and adjoint neutron flux obtained by the KAK in four neutron energy groups[6]

In the core, ℓ and β_{eff} are obtained as follows.

$$\ell = \frac{1}{H} \int_{Reactor} \left(\sum_g \phi_g^* \phi_g \frac{1}{v_g} \right) dV \qquad (20)$$

$$\beta_{eff} = \sum_h \sum_{K,K'} \beta_K a_{K'} W_{KK'} \qquad (21)$$

$$W_{KK'} = \frac{1}{H} \int_{Reactor} \left(\sum_{g'} \chi_{g'}^{K'} \phi_{g'}^* \sum_g F_g^K \phi_g \right) dV \qquad (22)$$

$$H = \int_{Reactor} \left(\sum_{g'} \chi_{g'} \phi_{g'}^* \sum_g F_g \phi_g \right) dV \qquad (23)$$

Here, H : normalization factor,

$W_{KK'}$: relative worths of various delayed-neutrons,

g,g' : indication of real and adjoint groups,

ϕ, ϕ^* : real and adjoint fluxes,

β_K : delayed-neutron fraction in isotope K,

$a_{K'}$: relative abundance of delayed neutron in delayed neutron group K' ; $\sum_{K'} a_{K'} = 1$,

v_g : average speed of neutron in group g,

χ : fission spectrum,

$\chi^{K'}$: spectrum of delayed-neutron group K'

F : ν times of the fission cross-section, and

F^K : ν times of fission cross-section of isotope K.

The data of Keepin's[14] were used for β_k and $a_{K'}$. The calculated delayed neutron fractions of each lattice are shown in Table 33. The calculated ℓ and β_{eff} are shown in Table 12 and in Fig.39 with the experimental results. Since the core of which water to fuel volume ratio was 1.77 was subcritical with 590 fuel rods, experimental β_{eff}/ℓ was estimated on the critical water level extraporated by inverse multiplication method, and the calculation was carried out about the core of which fuel rod array was 26 × 26. The calculations were performed by the same procedure also for the UO_2 lattices, and are compared with the PuO_2 - UO_2 lattices in Table 14 and Fig. 42. The descrepancies of calculated β_{eff}/ℓ from experimental results are less than 7 % and 5 % for the PuO_2 - UO_2 and UO_2 lattices respectively.

5. Conclusion

Critical experiments and analysis on the uniform 3.0 wt % PuO_2-natural UO_2 lattices were carried out over the range of the atomic number density ratio of H to Pu from 295 to 922. The fissile nuclides fraction of Pu was 75 wt %.

The followings are concluded briefly from the experimental and calculational results.

a) Maximum value of B_m^2 is at about 530 of H/Pu.

b) Horizontal reflector saving changes from 7.9 to 6.5 cm with H/Pu from 295 to 922.

c) Reactivity decrease by ^{241}Pu decay to ^{241}Am is about 1 dollar per year.

d) It should be noticed that by the spontaneous fission neutron, source level is too high to measure reactivity in low power level.

e) It was confirmed that the linear relation exists between the relation R_{Cd} - 1.0 and H/Pu.

f) The distributions of R_{Cd} - 1.0 show that the equiriblium neutron spectrum region exist at the inside of 2 lattice piches from core - reflector boundary.

g) β_{eff}/ℓ of PuO_2-UO_2 lattices are about 1/2 times of that of UO_2. It is due to the fact that β_{eff} are about 1/2 of UO_2 lattices.

h) The calculated K_{eff} had some dependence on the ratio of H/Pu. The differences between the calculated results and experimental ones ranged from - 0.24 to 0.70 % $\Delta K/K$ for the results using LASER and from 2.14 to 0.25 % $\Delta K/K$ for UGMG42-THERMOS.

i) The root mean square differences between the experimental and calculated thermal neutron densities ranged from 2 to 4 % in the core region. In the reflector region, the calculation underestimated by about 3 to 5 % for all lattices.

j) The calculated epi-thermal neutron flux agreeded with the epi-Cd Au activity by less than 2.5 % at core region, while the difference of them in reflector regions are 3 to 12 %.

k) The calculated power distributions agreeded good with the experimental results except the core boundary where the discrepancies were less than $\pm$ 5 %.

l) The calculated reactivity decrease due to the ^{241}Pu decay to ^{241}Am agreeded within the experimental error except one lattice.

m) The discrepancies of calculated β_{eff}/ℓ from experimental results are less than 7 % and 5 % for the P_uO_2-UO_2 and UO_2 lattices respectively. Noticeable changes are not observed about β_{eff} while β_{eff}/ℓ depend greatly on the water to

fuel volume ratio. The calculated prompt neutron-life time increases from 3.1×10^{-5} sec to 6.1×10^{-5} sec with H/Pu from 295 to 922.

Acknowledgements

The authors would like to express our thanks to Dr. K. Torikai, Dr. M. Ishizuka, Dr. S. Suguri, Mr. M. Osanai of JAERI and to Dr. H. Dr. Y. Nakamura, Dr. S. Suzuki of PNC for their continuous support and encouragement of this work. They are also grateful to Mr. M. Koizumi, Dr. Naruki and other members of the PNC for fabrication and inspection of the PuO_2-UO_2 fuel rods, and to Miss. S. Kozawa for her continuous effort of data handlings.

Reference

(1) " PLUTONIUM UTILIZATION IN COMMERCIAL POWER REACTOR," Nucl. Technol. Vol. 15 (1972).

(2) " A REVIEW OF PLUTONIUM UTILIZATION IN THERMAL REACTORS ," Nucl. Technol. Vol. 18 (1973).

(3) G.C.Hanna et. al., Atomic Energy Review, Vol. VII, NO.4, International Atomic Energy Agency, Vienna (1969).

(4) R.C.Liikala,V.O.Uotinen,U.P.Jenquin et.al., " Uncertainties in the analysis of plutonium fueled light water moderated assemblies," BNWL-1656 (1973).

(5) H.Tsuruta,S.Matsuura,I.Kobayashi,R.Yumoto,S.Kikuchi et. al., " Critical Experiments and Analyses on 7×7 PuO_2-UO_2 Lattices in Light-Water Moderated UO_2 Core," JAERI-1234 (1974).

(6) H.Tsuruta,K.Kitamoto " Experiments and Calculation of β_{eff}/ℓ for the Light-Water Moderated Two-Region core of $UO_2$and PuO_2 -UO_2 lattices, JAERI-M4696 (1972).

(7) R.Yumoto,S.Matsuura,et.al., " Critical Experiment and Analysis on Light Water Moderated 7×7 PuO_2-UO_2 Lattices," PNC- N841-71 -01 (1970).

(8) Poncelet C.G. : WCAP-6073 (1966).

(9) Katsuragi M., Horiguchi K. and Kuge Y. : JAERI-1104 (1966).

(10) B.J.Toppel and I.Baysys, " THE ARGONNE-REVISED THERMOS CODE," ANL-7023 (1965).

(11) W.R.Cadwell, P.F.Buerger,C.J.Pfeifer, " The PDQ·5 and PDQ·6 Programs for the Solution of the Two-Dimensional Neutron Diffusion-Depletion Problem," WAPD-TM-477 (1965).

(12) M.Akanuma,Y.Kuge,S.Yasukawa, " The KAK Program for the Numerical Solution of Few-Group Neutron Diffusion Equations in Two Dimensions," JAERI-1127 (1967).

(13) H.Tsuruta and K.Kobayashi," The Preparation of Input Data for KR302DPT," JAERI-memo 4775 (1972).

(14) Keepin G.R. ," Physics of Nuclear Kinetics," Addison-Wesley Publishing Co. Inc. (1965).

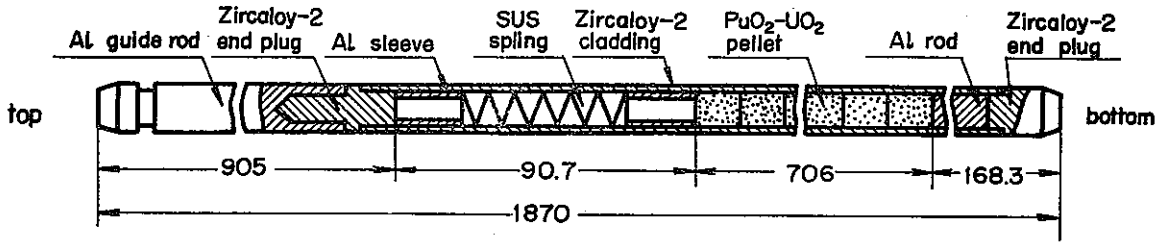

Fig. 1 3.0 wt % PuO_2-UO_2 fuel rod

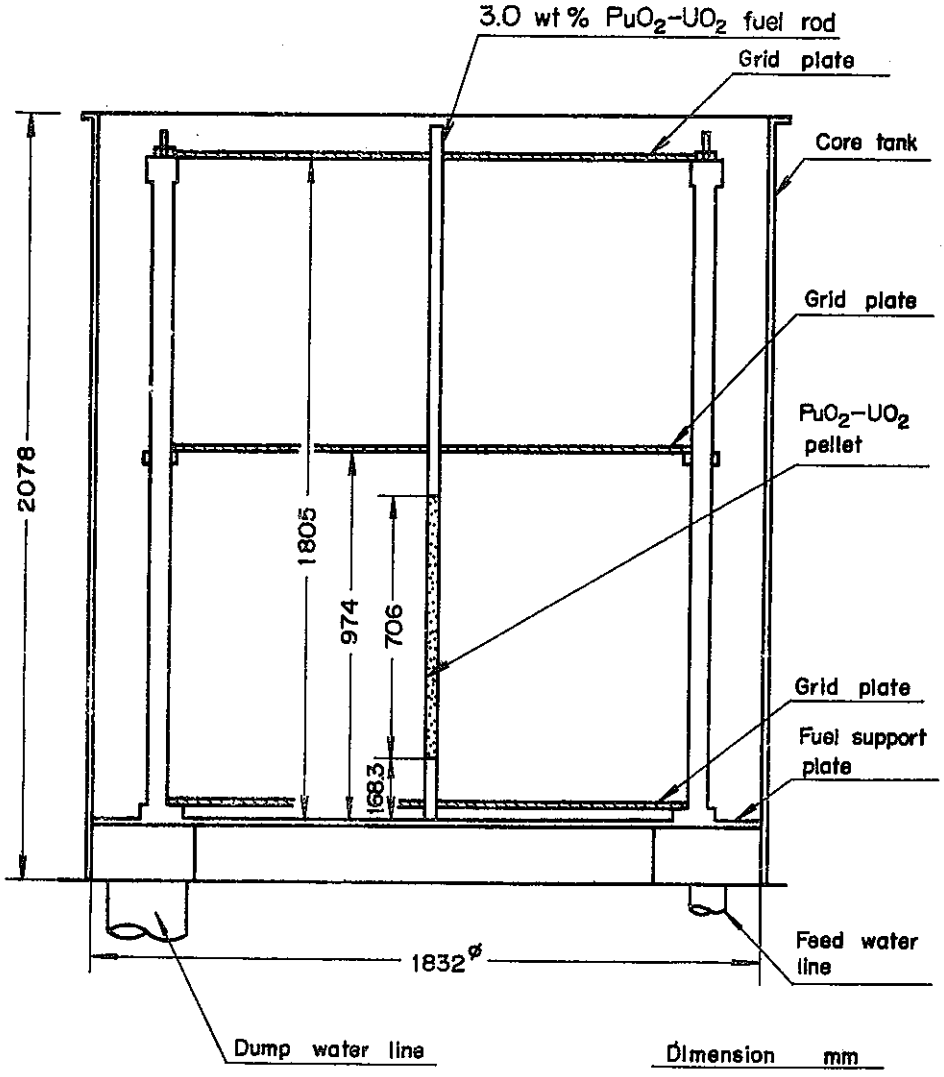

Fig. 2 Cross sectional view of core tank

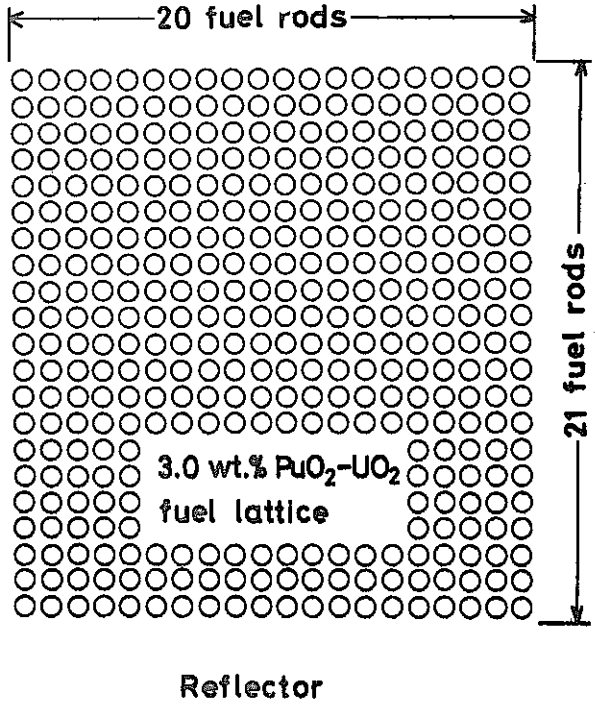

Fig. 3 Example of lattice configulation

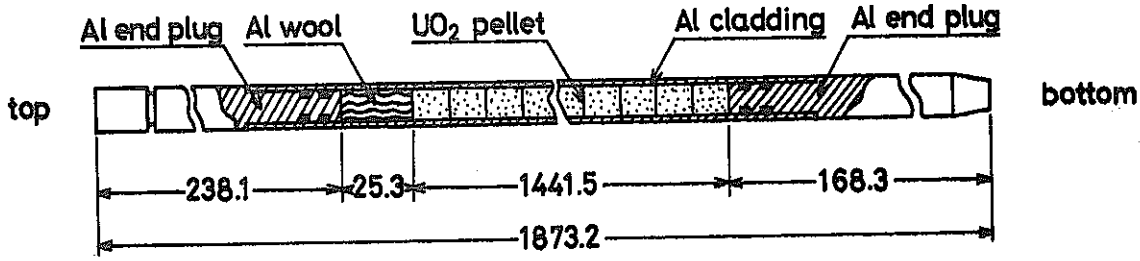

Fig. 4 2.6 wt % JP-II·UO_2 fuel rod

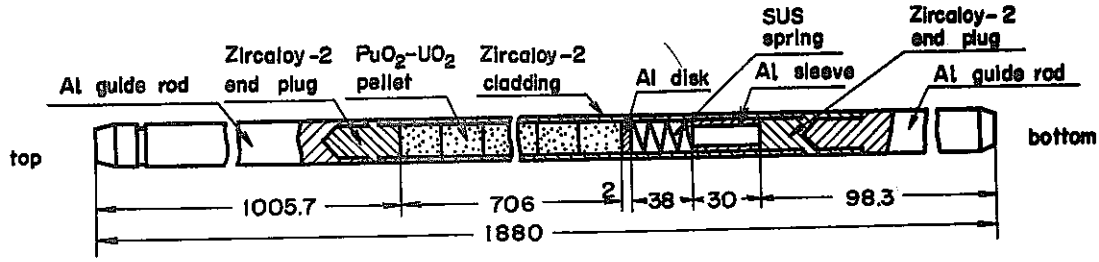

Fig. 5 3.4 wt % PuO_2-UO_2 fuel rod

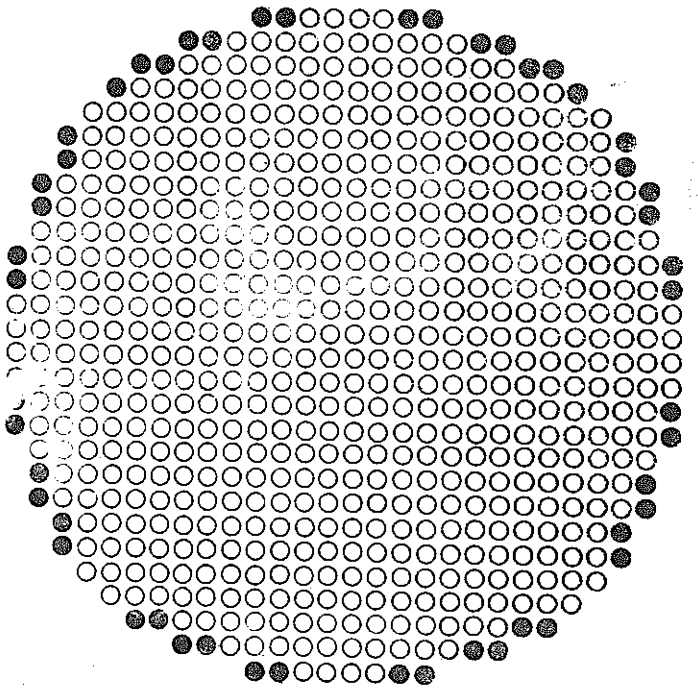

○ 3.0 wt.% PuO_2-UO_2

● 3.4 wt.% PuO_2-UO_2

Fig. 6 The plan view of the cylindrical core of which water to fuel volume ratio is 1.77

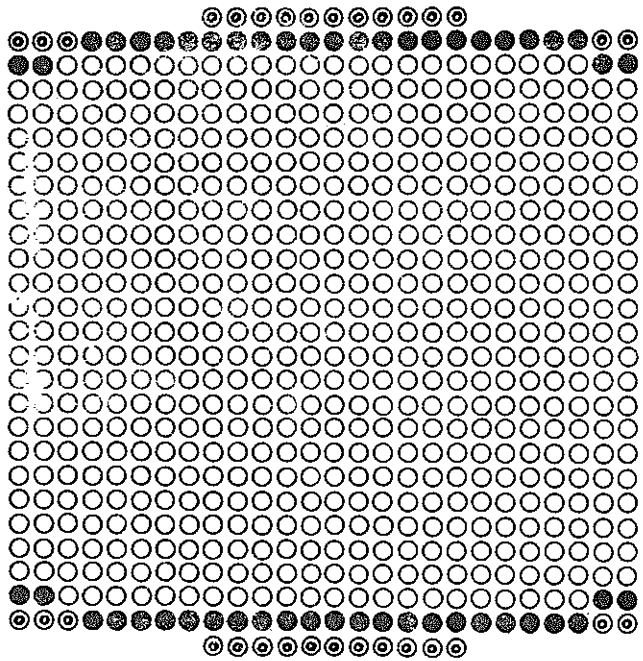

○ 3.0 wt.% PuO_2-UO_2

● 3.4 wt.% PuO_2-UO_2

◎ 2.6 wt.% JP-Ⅱ·UO_2

Fig. 7 The plan view of the square core of which water to fuel volume ratio is 1.77

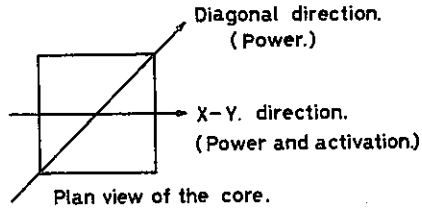

Fig.8 Diagonal and x-y directions in the core.

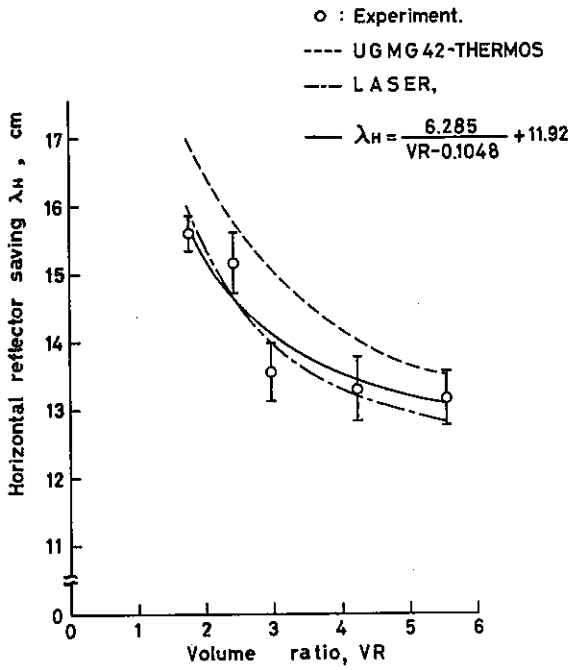

Fig. 9 Horizontal reflector saving vs. water to fuel volume ratio.

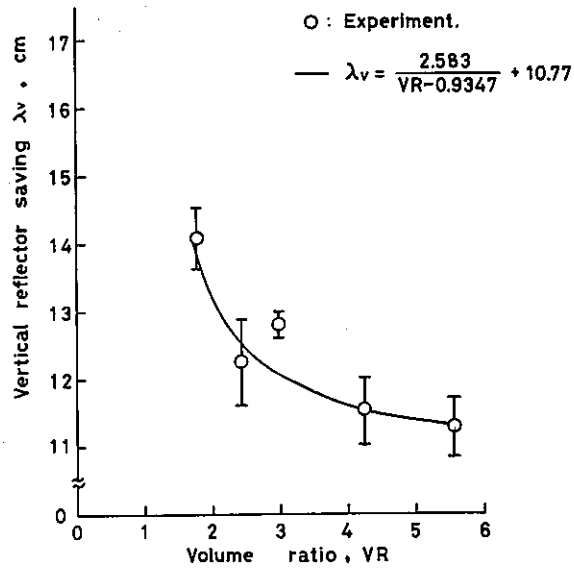

Fig. 10 Vertical reflector saving vs. water to fuel volume ratio.

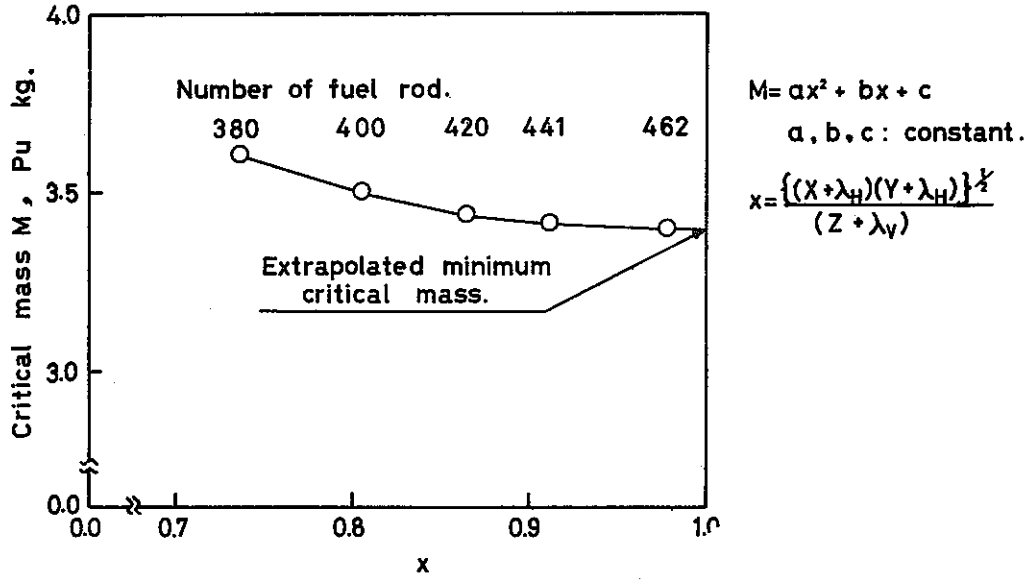

Fig. 11 Fitting of criticality data to quadratic curve.

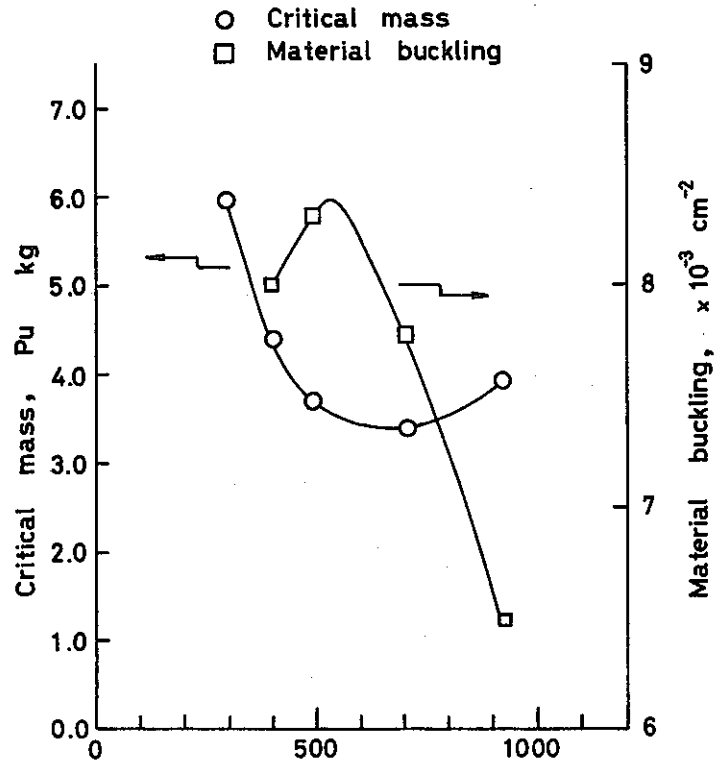

Fig. 12 Critical masses and material bucklings vs. H/Pu for the partially immersed cores.

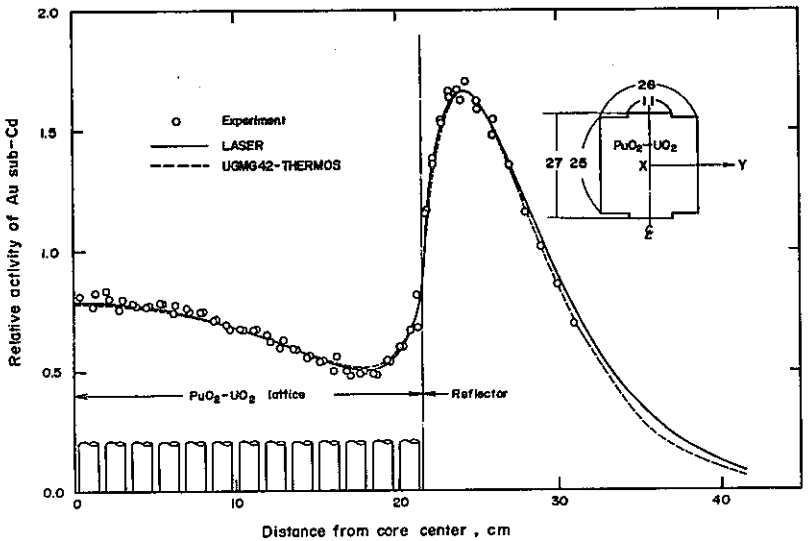

Fig. 13 Sub-Cd Au activity distribution of the lattice of which water to fuel volume ratio is 1.77

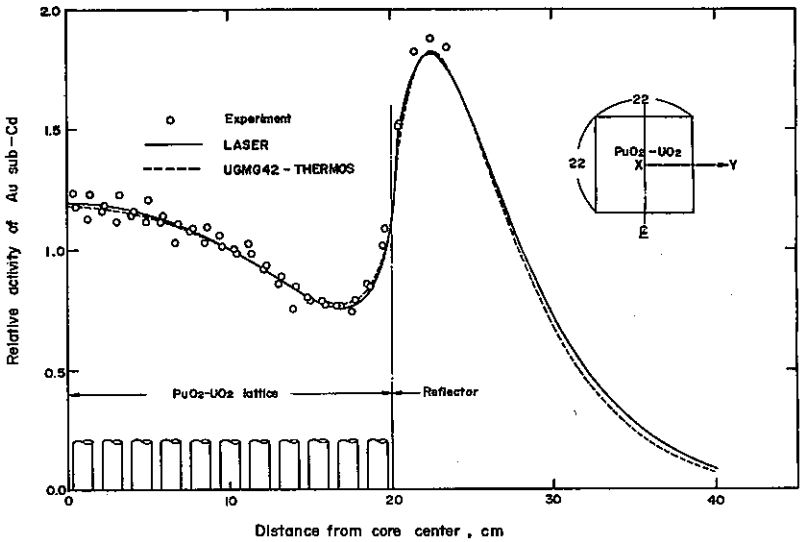

Fig. 14 Sub-Cd Au activity distribution of the lattice of which water to fuel volume ratio is 2.42

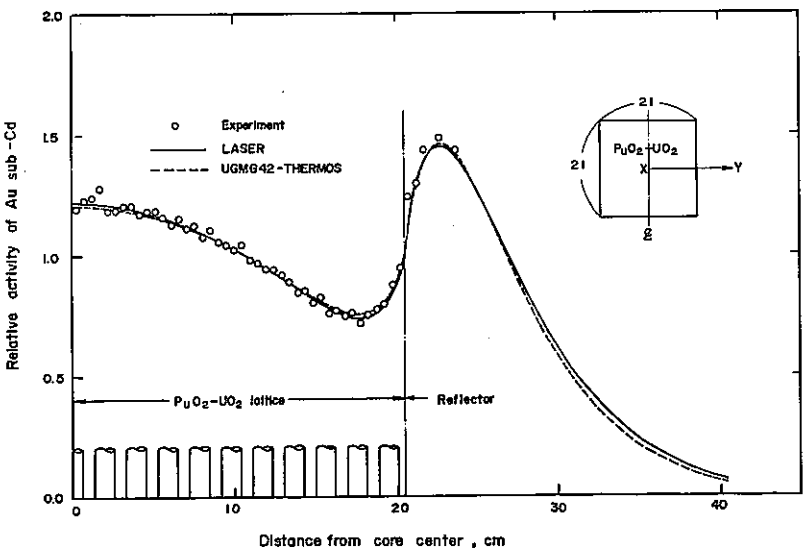

Fig. 15 Sub-Cd Au activity distribution of the lattice of which water to fuel volume ratio is 2.98

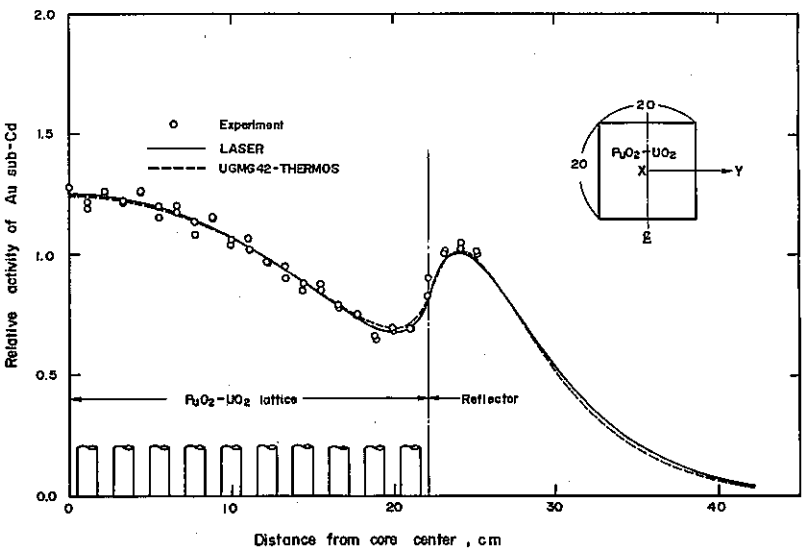

Fig. 16 Sub-Cd Au activity distribution of the lattice of which water to fuel volume ratio is 4.24

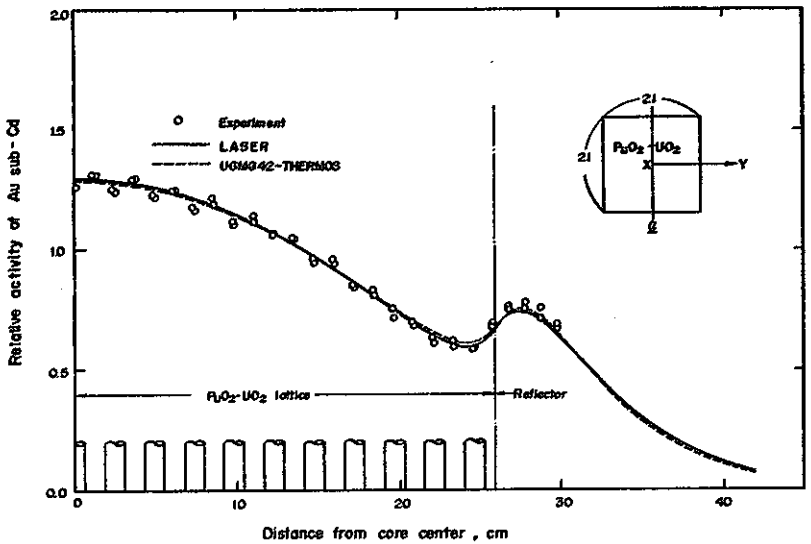

Fig. 17 Sub-Cd Au activity distribution of the lattice of which water to fuel volume ratio is 5.55

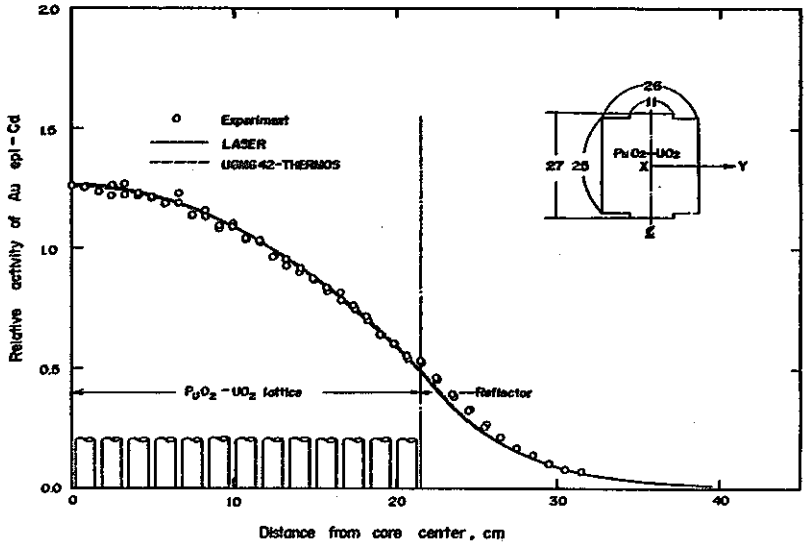

Fig. 18 Epi-Cd Au activity distribution of the lattice of which water to fuel volume ratio is 1.77

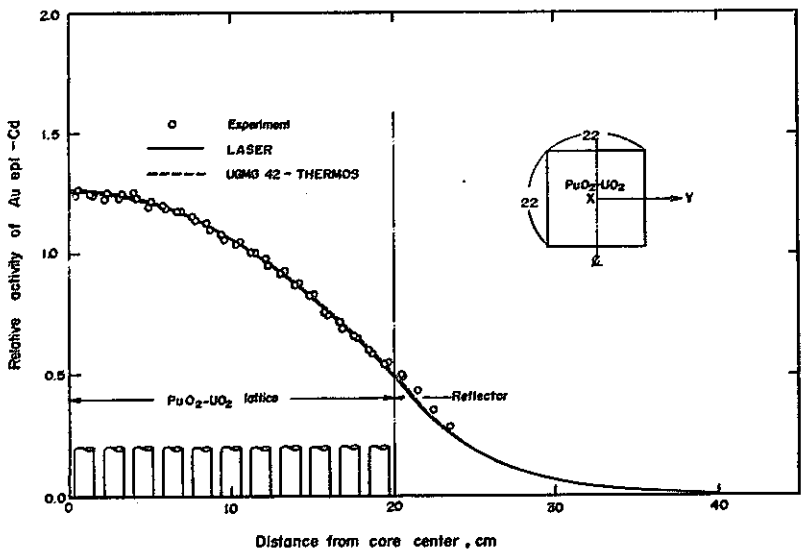

Fig. 19 Epi-Cd Au activity distribution of the lattice of which water to fuel volume ratio is 2.42

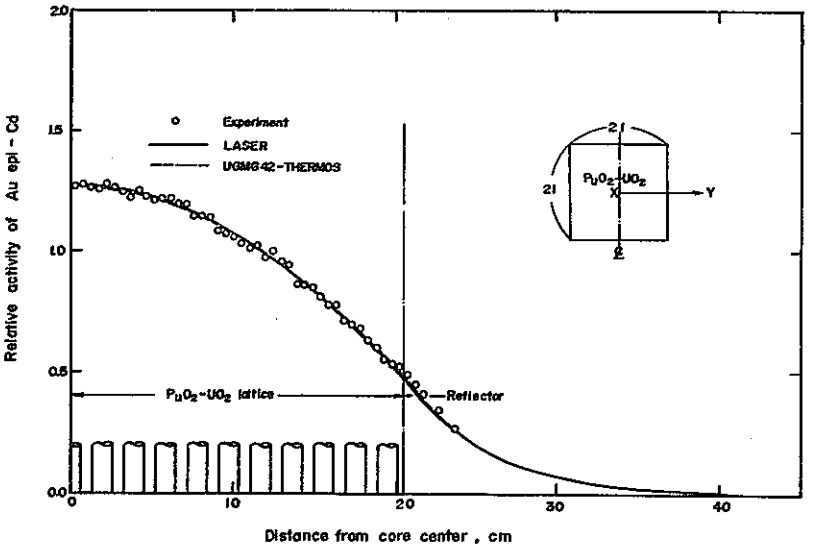

Fig. 20 Epi-Cd Au activity distribution of the lattice of which water to fuel volume ratio is 2.98

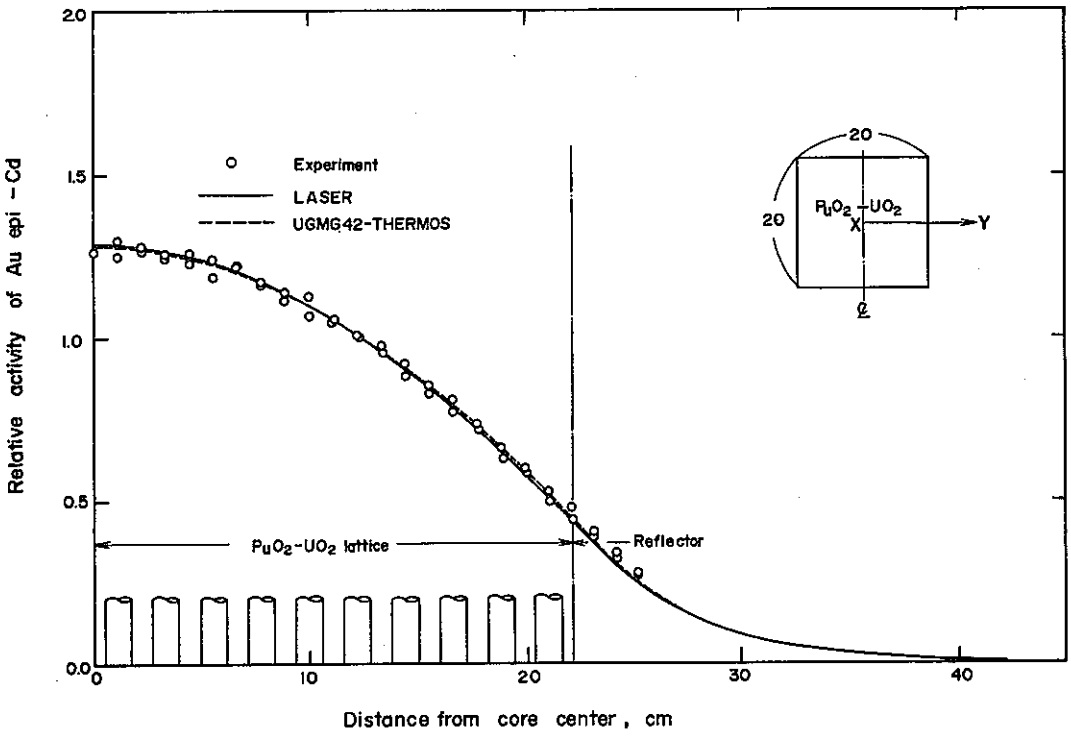

Fig. 21 Epi-Cd Au activity distribution of the lattice of which water to fuel volume ratio is 4.24

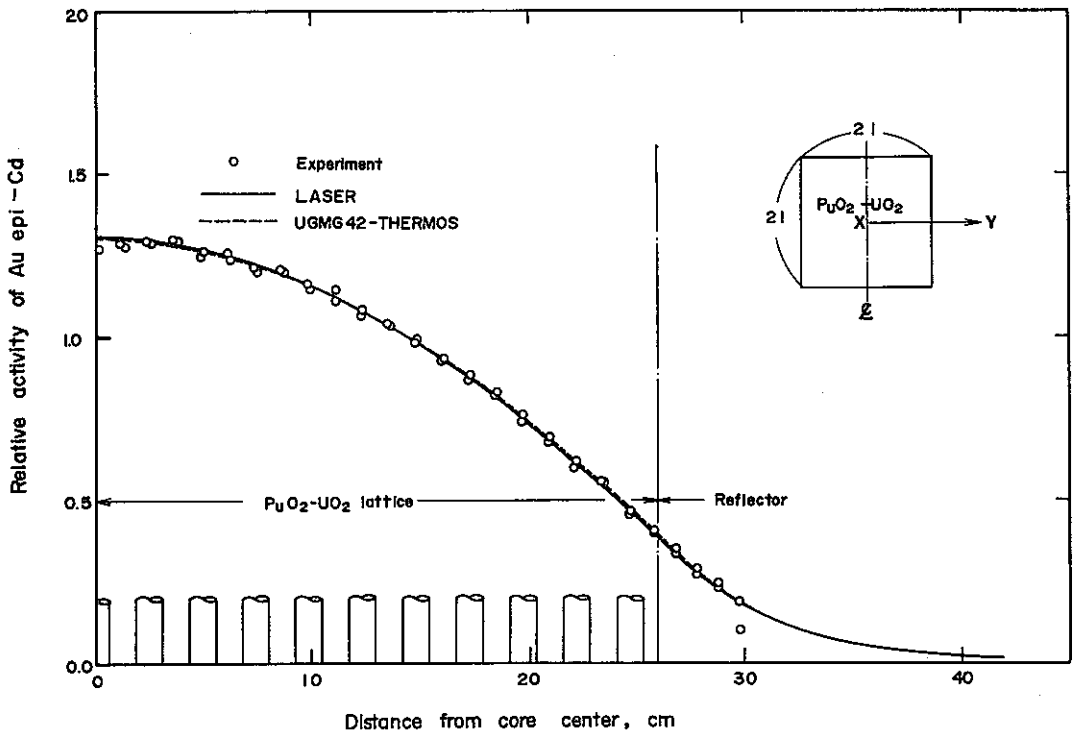

Fig. 22 Epi-Cd Au activity distribution of the lattice of which water to fuel volume ratio is 5.55

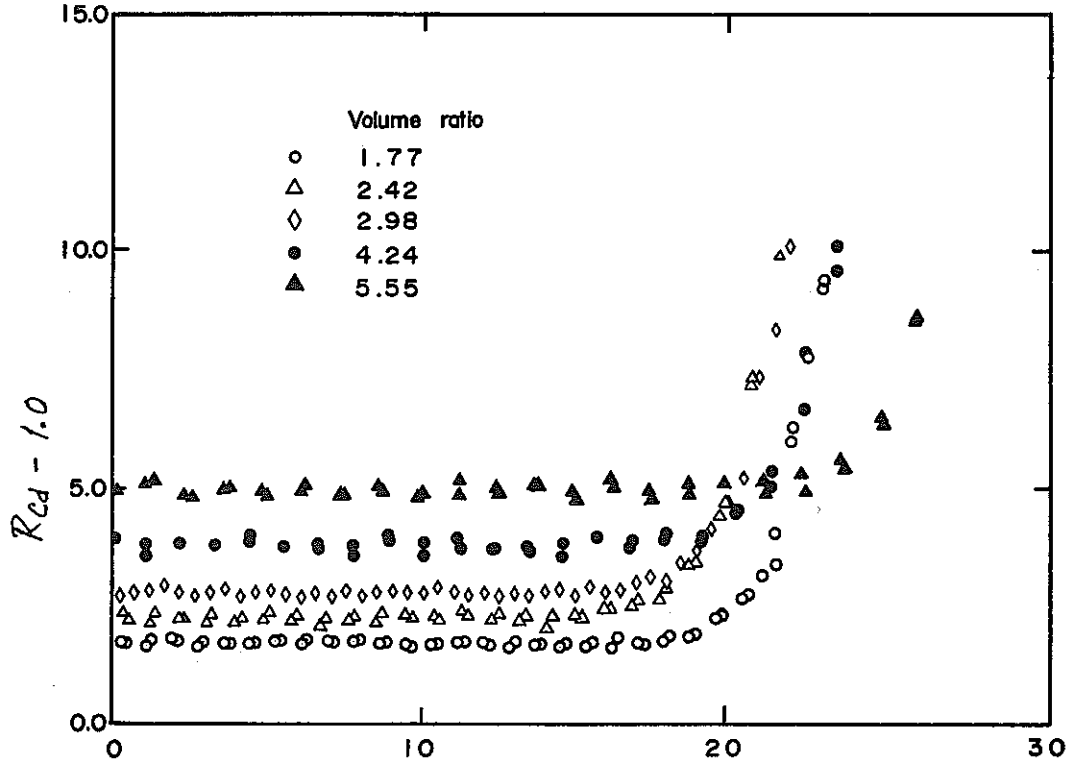

Fig. 23 R_{Cd}-1.0 vs. distance from core center

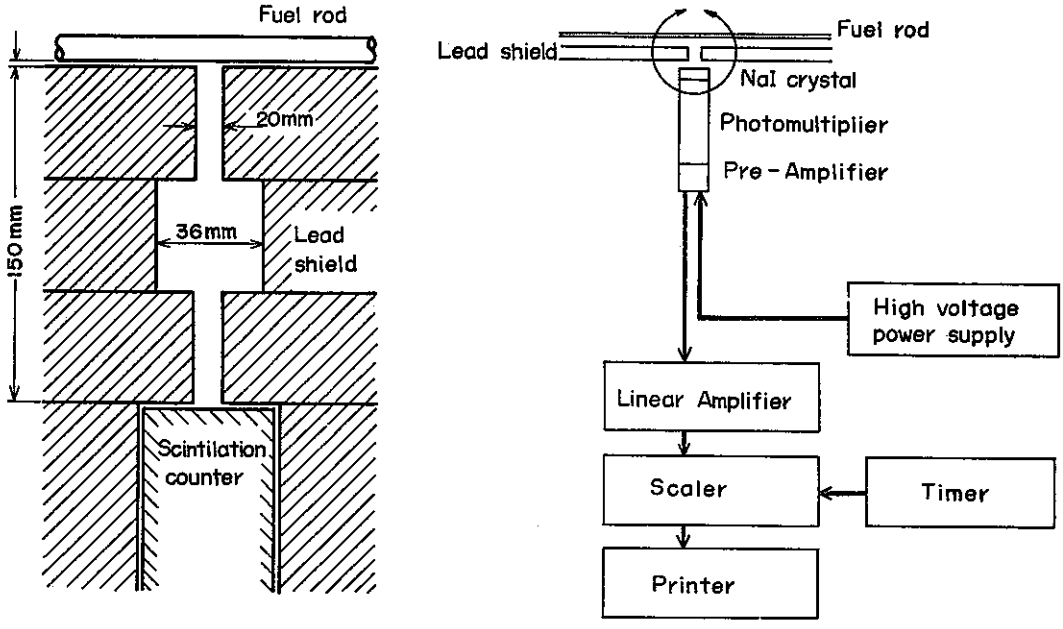

Fig. 24 Counting system of γ-rays from fission products.

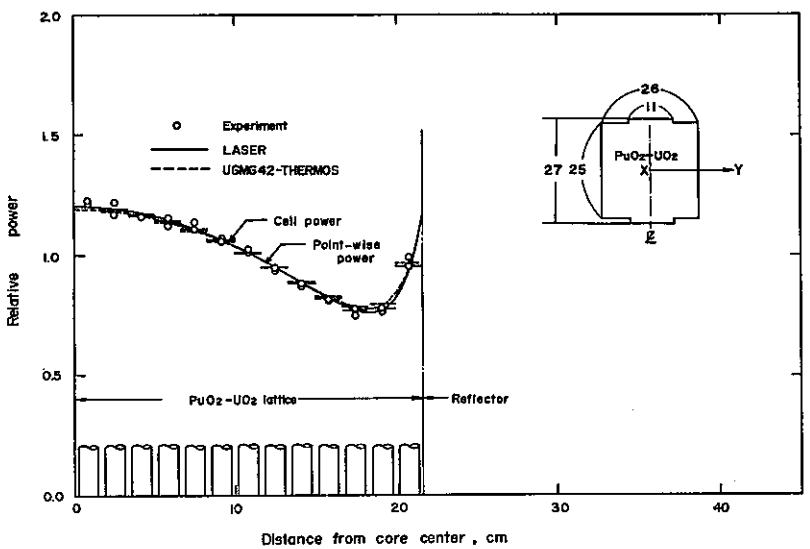

Fig. 25 Horizontal power distribution of the lattice of which water to fuel volume ratio is 1.77 (X-Y)

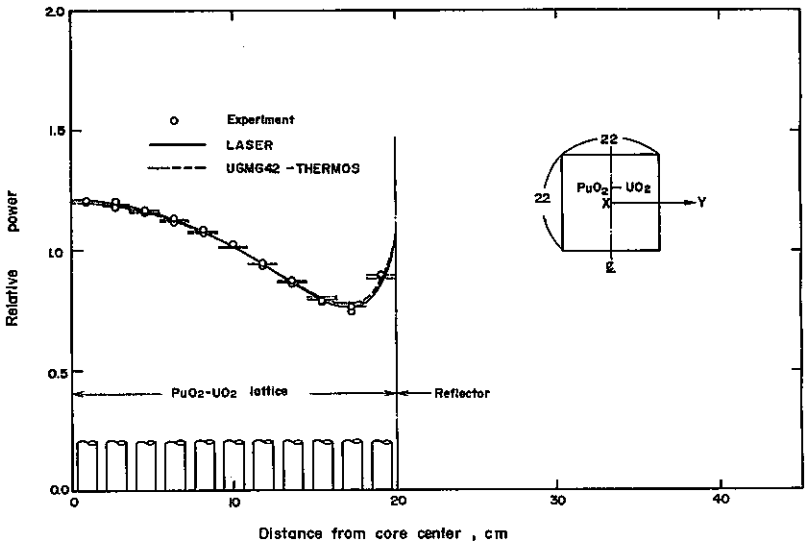

Fig. 26 Horizontal power distribution of the lattice of which water to fuel volume ratio is 2.42 (X-Y)

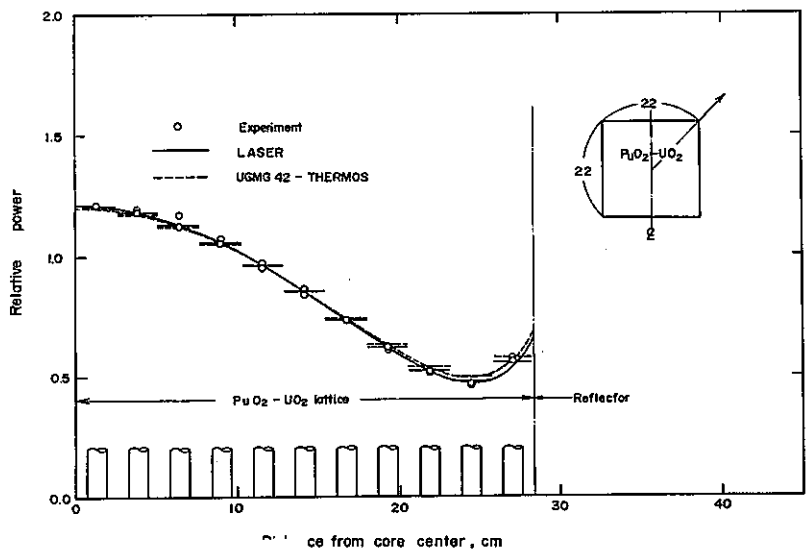

Fig. 27 Horizontal power distribution of the lattice of which water to fuel volume ratio is 2.42 (Diagonal)

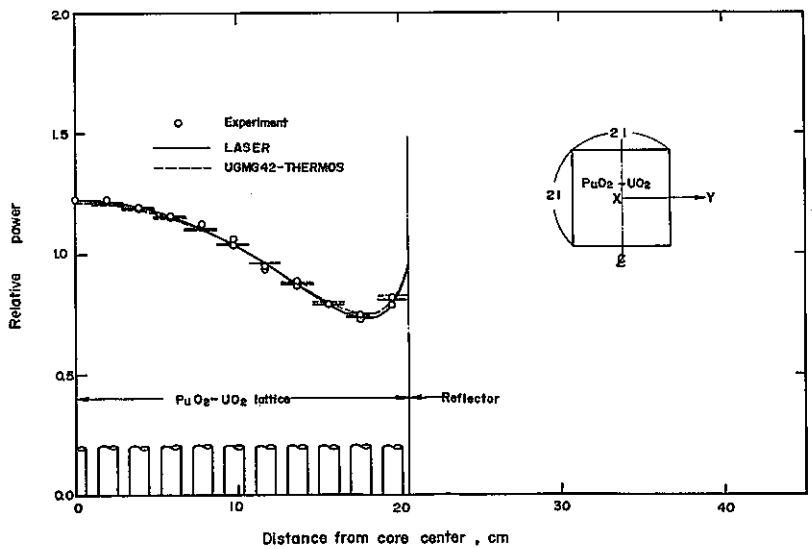

Fig. 28 Horizontal power distribution of the lattice of which water to fuel volume ratio is 2.98 (X-Y)

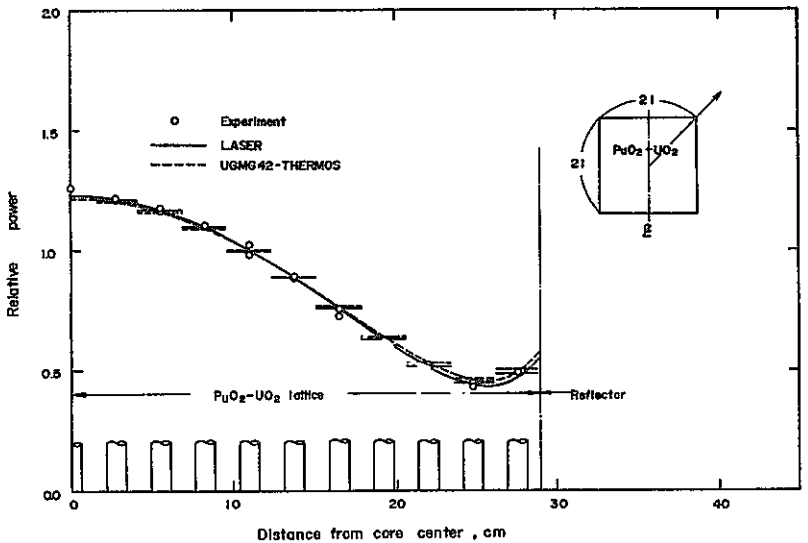

Fig. 29 Horizontal power distribution of the lattice of which water to fuel volume ratio is 2.98 (Diagonal)

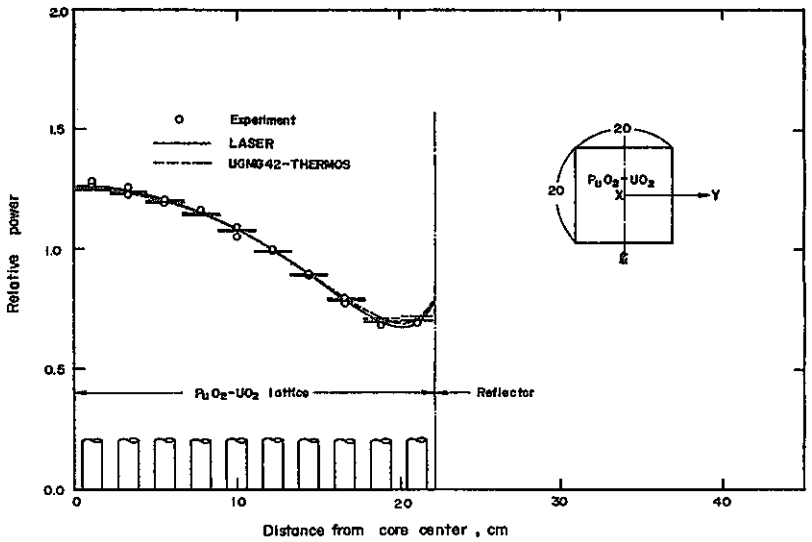

Fig. 30 Horizontal power distribution of the lattice of which water to fuel volume ratio is 4.24 (X-Y)

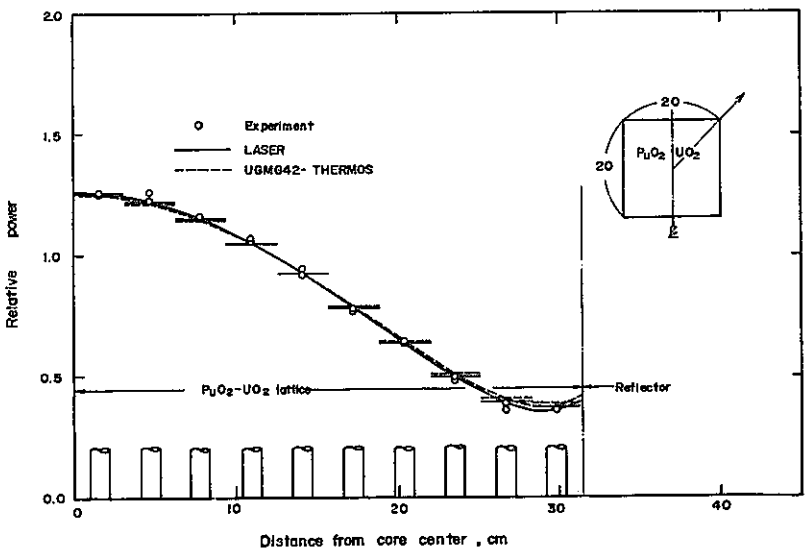

Fig. 31 Horizontal power distribution of the lattice of which water to fuel volume ratio is 4.24 (Diagonal)

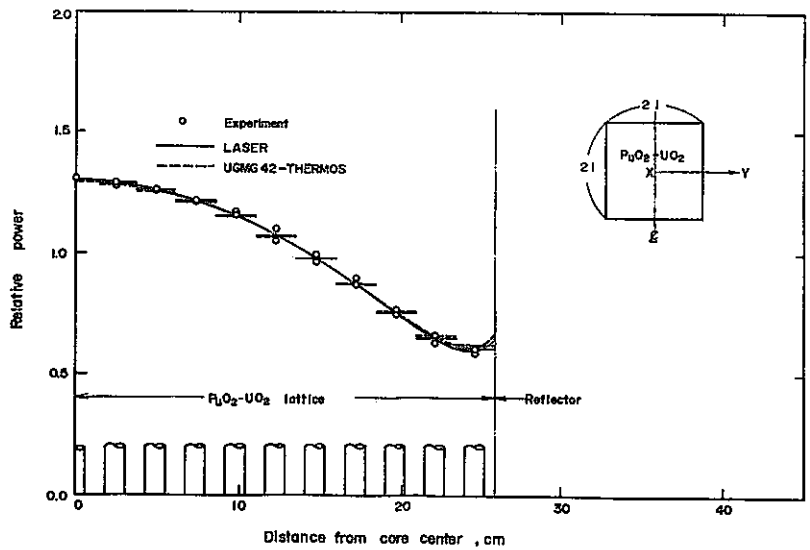

Fig. 32 Horizontal power distribution of the lattice of which water to fuel volume ratio is 5.55 (X-Y)

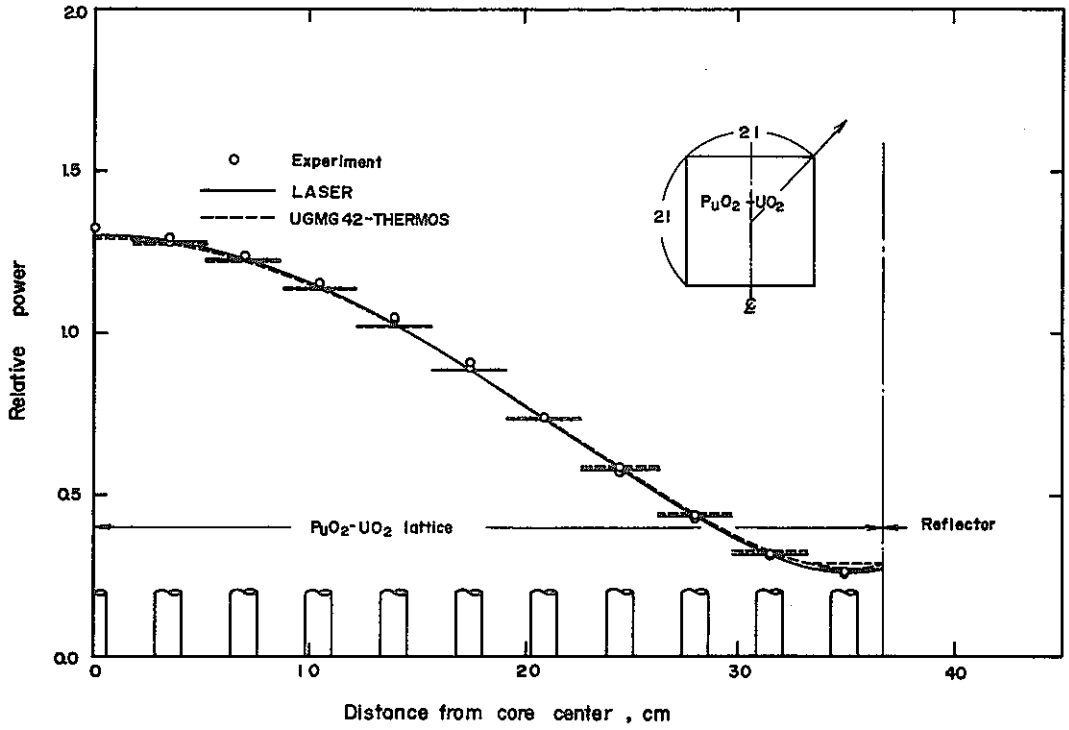

Fig. 33 Horizontal power distribution of the lattice of which water to fuel volume ratio is 5.55 (Diagonal)

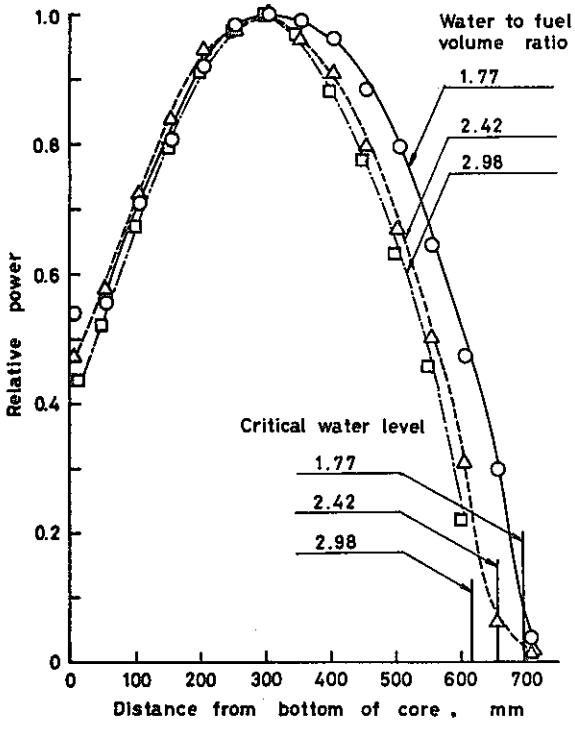

Fig. 34 Vertical power distribution for the lattices of which water to fuel volume ratios are 1.77, 2.42, and 2.98.

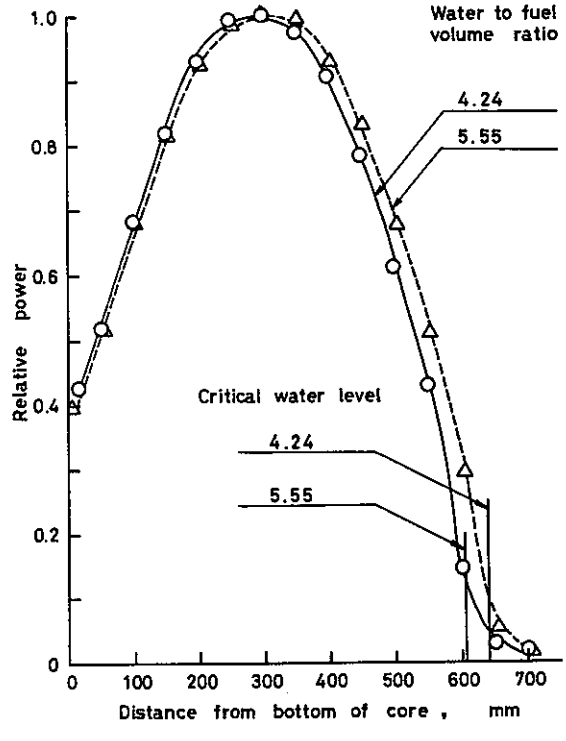

Fig. 35 Vertical power distribution for the lattices of which water to fuel volume ratios are 4.24 and 5.55.

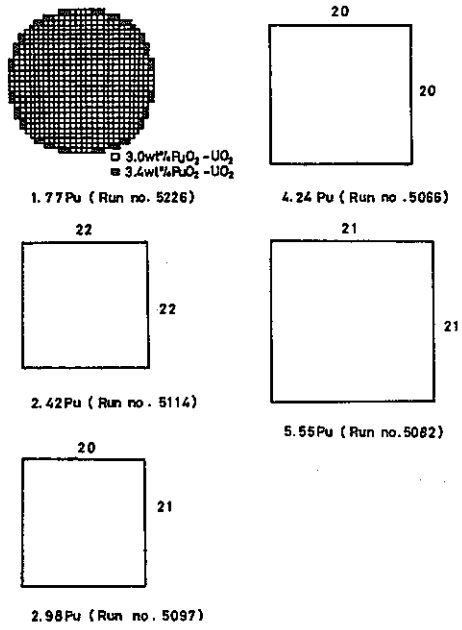

Fig. 36 Configurations of PuO_2-UO_2 lattices used for β_{eff}/l measerments.

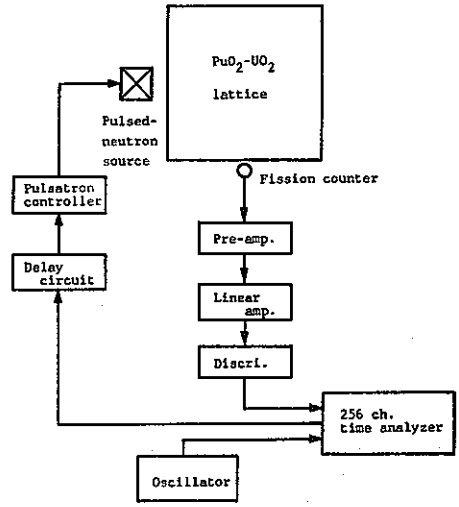

Fig. 37 Arrangement of pulsed-neutron experiment

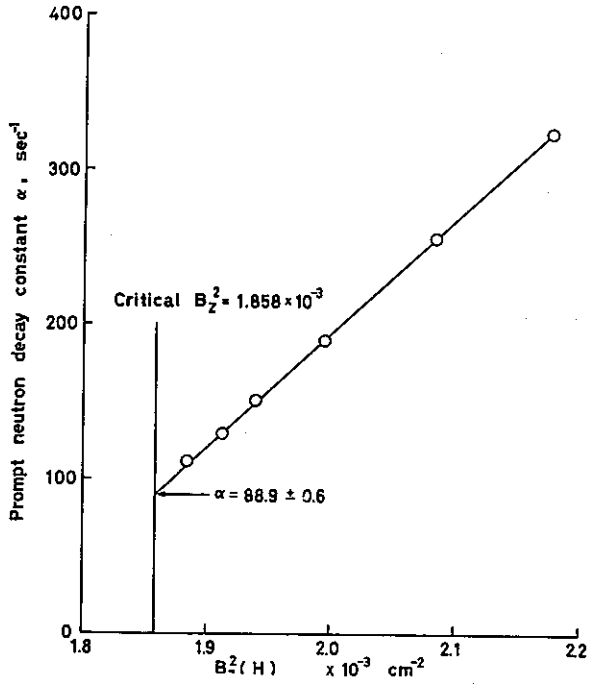

Fig. 38 Prompt neutron decay constant α vs. vertical buckling of the lattice of which water to fuel volume ratio is 2.98. The experimental error is included within the circle.

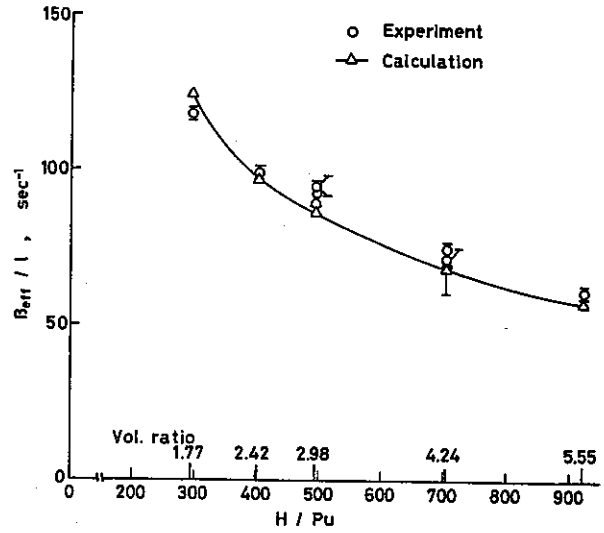

Fig. 39 The relation between β_{eff}/ℓ and H/Pu.

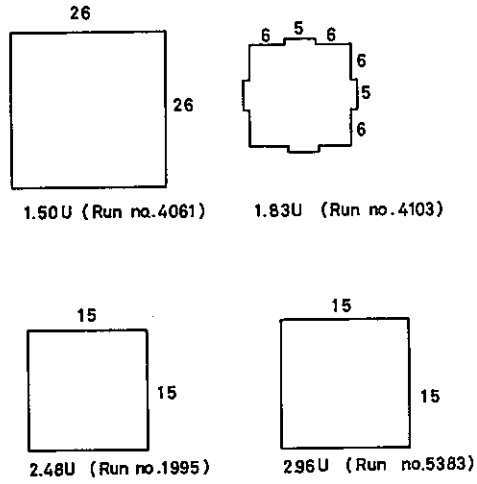

Fig. 40 Configuration of UO_2 fuel cores

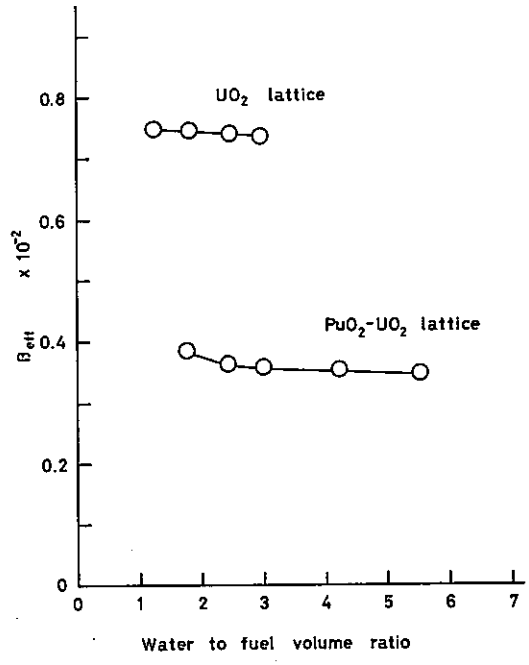

Fig. 41 Relation between β_{eff} and water to fuel volume ratio.

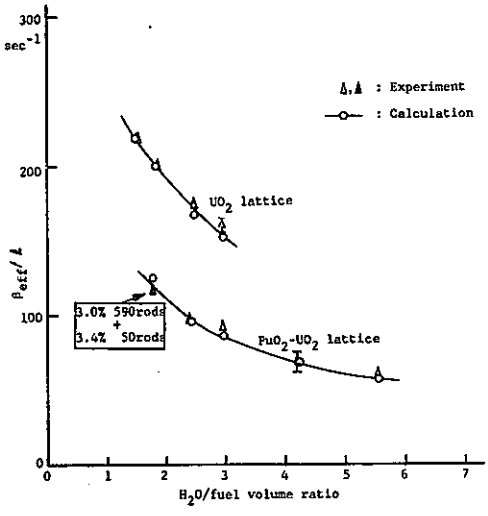

Fig.42 The relation between β_{eff}/ℓ and the volume ratio

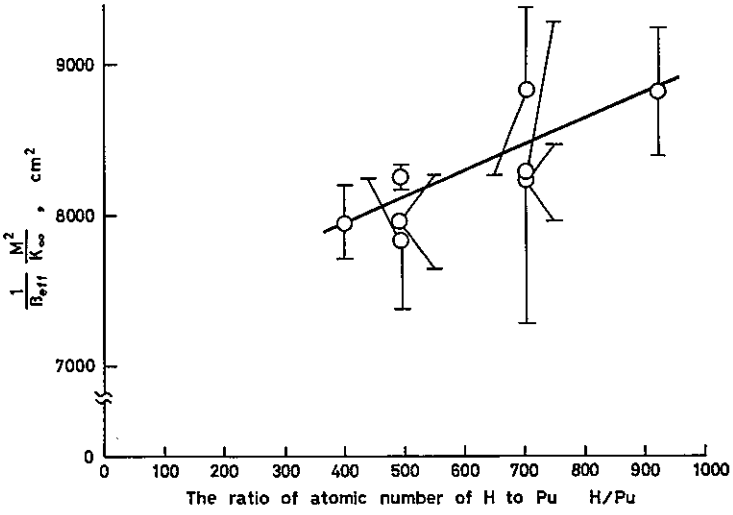

Fig. 43 The relation between $\frac{1}{\beta_{eff}} \frac{M^2}{K_\infty}$ and $\frac{H}{Pu}$

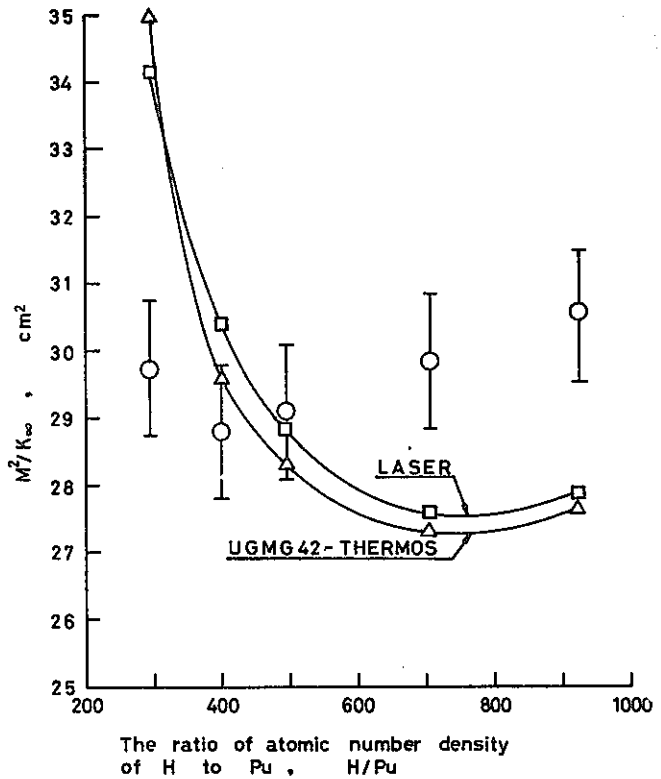

Fig. 44 M^2/K_∞ vs. H/Pu

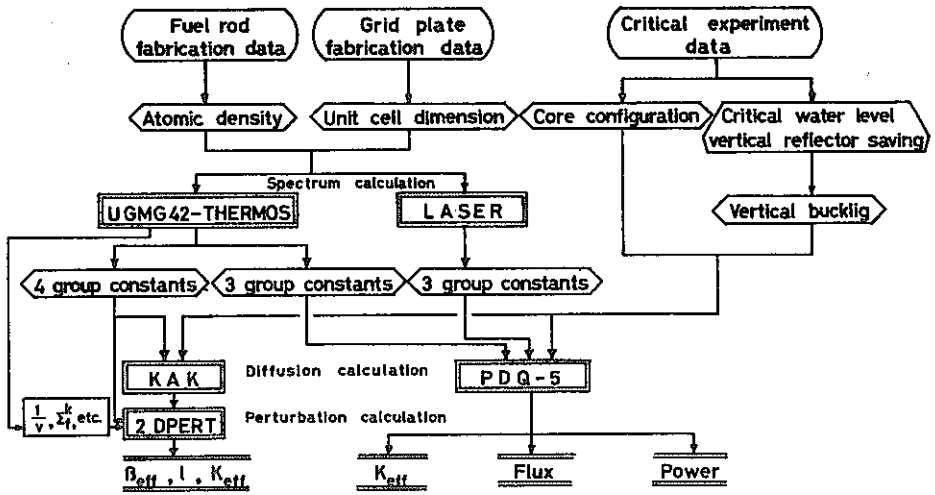

Fig. 45 Calculational scheme.

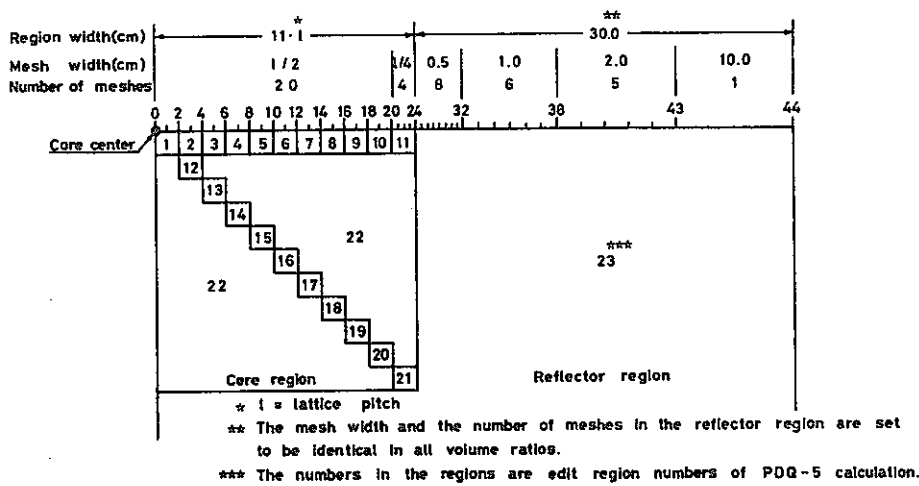

Fig. 46 Mesh spaces in two dimensional diffusion calculation of the lattice of which water to fuel volume ratio is 2.42.

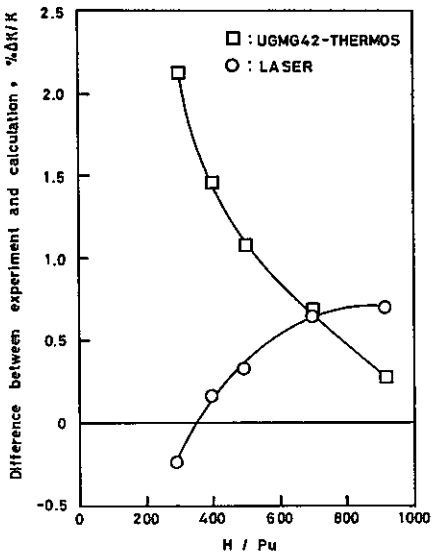

Fig. 47 K_{eff} difference between experiment and calculation ($\frac{\text{cal.} - \text{exp.}}{\text{exp.}}$) vs. H/Pu .

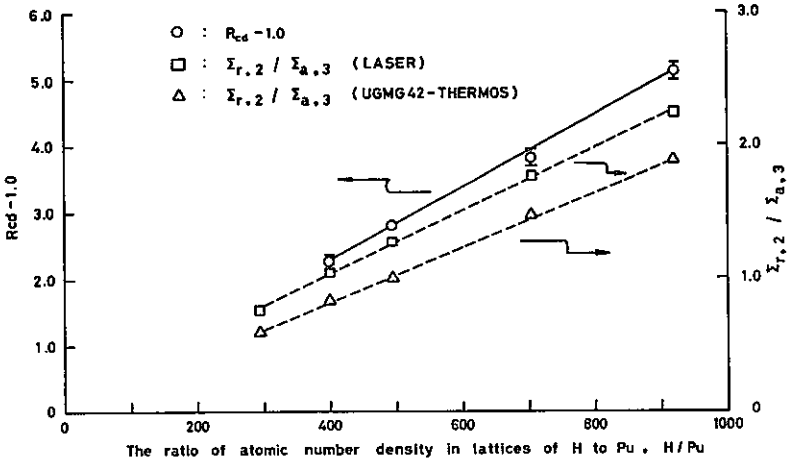

Fig. 48 The linear relation of R_{Cd}-1.0 or $\Sigma_{r,2}/\Sigma_{a,3}$ with H/Pu

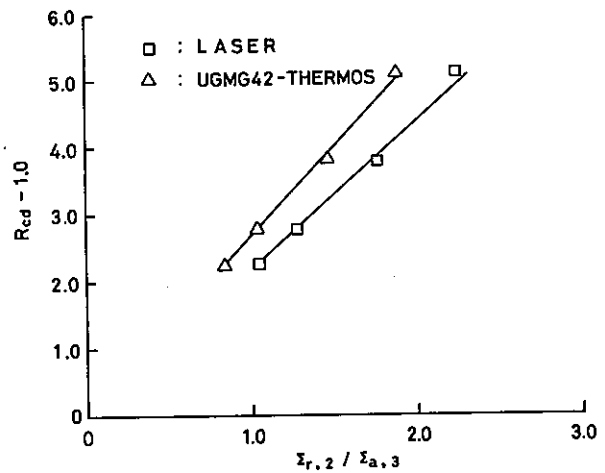

Fig. 49 The linear relation of R_{Cd} - 1.0 with $\Sigma_{r,2}/\Sigma_{a,3}$.

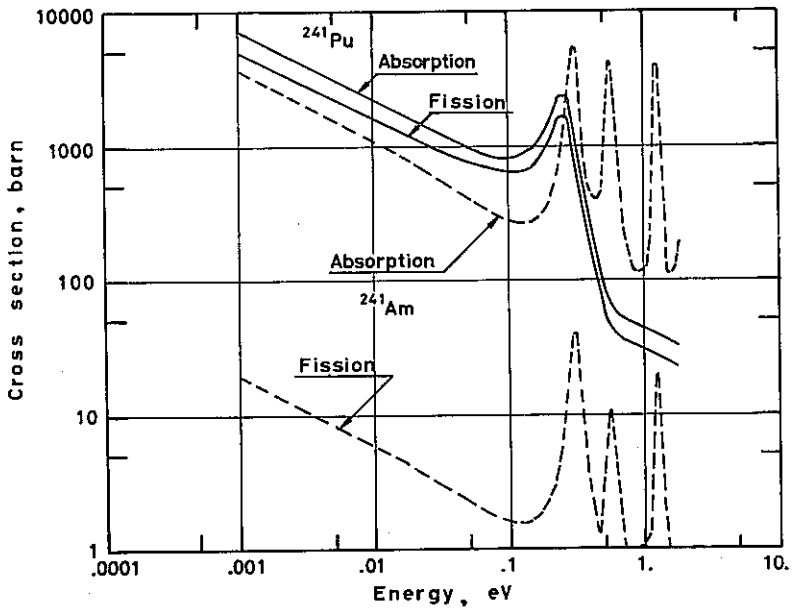

Fig. 50 Cross-section of ^{241}Am and ^{241}Pu.

Table 1. Fuel fabrication data of 3.0 wt% PuO_2-UO_2

Fuel pellet	
Fabrication method	Mechanically blended and pre-sintered
Uranium composition	Natural uranium
Plutonium enrichment $PuO_2/(PuO_2-UO_2)$	3.01 ± 0.05 wt%
Plutonium composition	
Date of assay	August 19, 1971
^{238}Pu	0.494 wt %
^{239}Pu	68.18
^{240}Pu	22.02
^{241}Pu	7.26
^{242}Pu	2.04
Americium content*)	
Date of assay	August 16, 1971
^{241}Am	530 ppm
Inpurity content**)	
Equivalent boron concentration	0.90 $^{+0.09}_{-0.12}$ ppm
O/M	2.07
Pellet density	6.056 ± 0.076 g/cm^3
Pellet diameter	10.65 mm
Stack length ***)	706 ± 3 mm
Stack weight	
PuO_2-UO_2	380.6 g
Pu total	10.06
^{239}Pu + ^{241}Pu	7.61
^{235}U	2.30
Cladding	
Material	Zircaloy-2
Inner diameter ***)	10.83 ± 0.06 mm
Thickness ***)	0.70 ± 0.07 mm

*) Relative value to pultonium dioxide.
**) Relative value to mixed oxide.
***) Value of specification.

Table 2. Description of cores

Core name	1.77 Pu	2.42 Pu	2.98 Pu	4.24 Pu	5.55 Pu
Lattice pitch cm	1.660	1.825	1.956	2.225	2.474
water to fuel volume ratio	1.77	2.42	2.98	4.24	5.55
Number of fuel rods at critical	See Appendix 1	22x22 22x23 23x23 23x24 24x24	20x21 21x21 21x22	19x20 20x20 20x21 21x21 21x22	20x21 21x21 21x22
Geometrical shape of core		rectangular prism			

Table 3. Temperature reactivity coefficient at 20°C

Water to fuel volume ratio	H/Pu	Temperature coefficient Cent/°C
2.42	402	-0.773
2.98	494	-0.148
4.24	704	1.25
5.55	922	3.43

Table 4. Criticality data and reactivity decrease due to ^{241}Pu decay to ^{241}Am

Criticality data				Reactivity decrease rate				
Water to fuel volume ratio	Fuel rod array	Date	Critical water level mm	Time interval day	Core temp. °C	Reactivity decrease Cent	Reactivity decrease rate Cent/day	Average Cent/day
2.42	22x22	June 6 '72	693.8		18.7			
		May 14 '73	Sub-critical	342	18.0			
	22x23	June 7 '72	639.8		19.1			
		Nov. 8 '72	652.6	154	18.9	43.7±3.5	0.284	
	23x23	June 7 '72	595.3		19.1			
		May 14 '73	618.6	341	18.7	93.5±7.5	0.274	
	23x24	June 7 '72	562.5		19.2			
	24x24	June 7 '72	532.9		19.7			
		May 14 '73	550.0	341	18.7	91.3±7.3	0.268	0.28 ± 0.02
2.98	20x21	May 18 '72	670.9		17.5			
		May 22 '73	Sub-critical	369	19.3			
	21x21	May 18 '72	614.9		17.6			
		May 22 '73	643.9	369	19.9	106.4±8.5	0.288	
	21x22	May 18 '72	573.7		17.8			
		May 22 '73	598.8	369	20.0	110.0±8.8	0.298	0.29 ± 0.02
4.24	19x20	Apr.13 '72	656.9		13.2			
		May 29 '73	686.9	411	19.6	106.1±8.5	0.258	
	20x20	Apr.13 '72	605.6		13.2			
		May 29 '73	630.2	411	19.8	107.7±8.6	0.262	
	21x21	Apr.14 '72	535.9		13.0			
		May 29 '73	554.9	410	19.8	113.5±8.3	0.277	0.27 ± 0.02
5.55	20x21	Apr.26 '72	664.0		16.2			
		June 6 '73	690.9	406	20.7	101.7±8.1	0.250	
	21x21	Apr.28 '72	622.1		18.0			
		June 6 '73	644.4	404	20.8	101.1±8.1	0.250	
	21x22	Apr.26 '72	589.8		16.4		0	
		June 6 '73	610.4	406	20.8	114.3±9.1	0.282	0.26 ± 0.02

Table 5. Reactor period and reactivity relation

unit : Cent

Reactor period sec \ Water to fuel volume ratio	2.42	2.98	4.24	5.55
30	23.51	23.63	23.80	23.91
50	17.03	17.11	17.25	17.33
100	10.27	10.32	10.41	10.46
200	5.79	5.82	5.87	5.90
300	4.04	4.06	4.10	4.12
- 10	-41.94	-42.26	-42.72	-42.00
-200	- 8.34	- 8.39	- 8.47	- 8.51
-300	-5.12	- 5.15	- 5.20	- 5.22
-400	-3.70	- 3.72	- 3.76	- 3.78

Table 6. Neutron emission from PuO_2-UO_2

	Weight of isotope g/g(PuO_2-UO_2)	Spontaueous neutron n/g(PuO_2-UO_2)	Weight of oxide g/g(PuO_2-UO_2)	(α,n) neutron n/g(PuO_2-UO_2)
^{238}Pu	0.000130	3.367×10^{-1}	0.000148	2.072
^{239}Pu	0.018086	5.281×10^{-4}	0.020588	9.265×10^{-1}
^{240}Pu	0.005841	5.362	0.006649	1.130
^{241}Pu	0.001860		0.002118	
^{242}Pu	0.000540	9.504×10^{-1}	0.000615	1.661×10^{-3}
Pu total	0.02646	6.650	0.03012	4.130
^{235}U	0.006052	1.404×10^{-6}	0.006895	7.171×10^{-6}
^{238}U	0.845259	1.665×10^{-1}	0.962929	1.425×10^{-4}
U total	0.85136	0.1665	0.96988	1.497×10^{-4}
Tatal Pu, U		6.817		4.130

Neutrons from spontaneous fission and (α,n) reaction of oxigen per a fuel rod is

$$(6.8 + 4.1) \times 380 = 4.14 \times 10^3 \text{ n/sec.}$$

Table 7 Specification of additionally loaded fuels

January 1969

Fuel	3.4 wt% PuO_2-UO_2	2.6 wt% JP-II UO_2
Fuel type	pre-sintered pellet	sintered pellet
Pellet diameter,cm	1.070	1.071
Fuel lenght,cm	70.6	144.15
Clad I.D.,cm	1.084	1.083
Clad thickness,cm	0.070	0.070
Clad material	Zircaloy-2	Aluminium
Pellet density,g/cm^3	6.824 (62.17 % T.D.)	10.41
$PuO_2/(PuO_2+UO_2)$,wt%	3.37	
Average Pu composition,wt%		
^{238}Pu	0.01	
^{239}Pu	90.64	
^{240}Pu	8.46	
^{241}Pu	0.84	
^{242}Pu	0.05	
Uranium enrichment,wt%		
^{234}U	0.0058	
^{235}U	0.713	2.588
^{238}U	99.2812	97.412

Table 8 Description of cores

Core pattern		Cylinder	Square
Date		Sep.27,'72	Oct.17,'73
Number of fuel rods at critical	3.0% PuO_2-UO_2	590	590
	3.4% PuO_2-UO_2	50	50
	2.6% UO_2	0	32
Core temperature,°C		21.3	21.0
Critical water level,cm		68.79	66.12
Lattice pitch,cm		1.660	
Water to fuel volume ratio		1.77	

Table 9 Reflector savings

Water to fuel volume ratio	1.77	2.42	2.98	4.24	5.55
Horizontal reflector savings λ_H ;					
by power distributions					
x - y direction	15.2±0.9	15.8±0.5	14.1±0.6	12.7±0.8	13.7±0.5
	15.5±0.4			12.6±0.7	13.0±0.7
diagonal distribution		14.7±0.4	13.2±0.4	13.0±0.4	12.6±0.3
				13.8±0.4	13.4±0.4
by epi-Cd Au activation distributions					
x - y direction	15.7±0.4	15.2±0.5	13.9±0.6	13.5±0.6	13.6±0.7
					13.4±0.3
Average	15.6±0.3	15.2±0.5	13.5±0.4	13.3±0.5	13.2±0.4
Fitted values by the equation*	15.7±0.3	14.6±0.3	14.1±0.3	13.4±0.2	13.1±0.2
Vertical reflector savings λ_V**					
by power distribution	14.5±0.9	11.9±0.2	12.8±0.5	11.9±0.4	11.1±0.3
	14.6±1.0	11.8±0.3	13.0±0.4	11.4±0.5	11.1±0.3
	13.7±0.7	13.0±0.4	12.5±0.5	11.3±0.3	11.7±0.4
		12.3±0.6			11.2±0.5
		12.2±0.4			12.1±0.8
		13.5±0.8			11.7±0.6
Average	14.1±0.4	12.2±0.6	12.8±0.2	11.5±0.3	11.3±0.4
Fitted values by the equation*	13.9±0.6	12.5±0.2	12.0±0.2	11.6±0.2	11.3±0.2

* Reflector saving are fitted to the equation $\lambda_{H,V} = \frac{b}{VR - a} - c$ where $\lambda_{H,V}$ is measured reflector savings, VR is water to fuel volume ratio, and a,b,c are constants.

** Partially immersed core in water.

Table 10 Minimum critical masses and material buklings of partially immersed cores.

May 16, 1972

Water to fuel volume ratio	Atomic number ratio H/Pu	Minimum critical mass Pu Kg	Material buckling $\times 10^{-3}$ cm^{-2}
1.77	295	5.94	
2.42	402	4.39	8.064 0.005
2.98	494	3.69	8.311 0.006
4.24	704	3.40	7.782 0.002
5.55	922	3.93	6.491 0.004

Table 11 Description of lattices

Water to fuel volume ratio	1.77	2.42	2.98	4.24	5.55
Critical water level (cm)	69.36	69.68	67.20	60.87	62.36
Fuel rod array	cylinder	22×22	20×21	20×20	21×21
Number of fuel rods at critical	3.0 - 590 3.4 - 50	484	420	400	441

Table 12 Measured and calculated results of β_{eff}/ℓ and K_{eff}

Water to fuel volume ratio	H/Pu	Fuel rod array	Critical water level (cm)	Neutron counter (2)	Measured		Calculated				Difference (3)	
					K_{eff} (4)	β_{eff}/ℓ sec^{-1}	K_{eff}	β_{eff}/ℓ sec^{-1}	ℓ $\times10^{-5}$sec	β_{eff} $\times10^{-2}$	K_{eff} %⊿K/K	β_{eff}/ℓ %
1.77 (1)	295	26×26		FC 4		118.2 1.6		124.3	3.094	0.3846		5.2
2.42	402	22×22	69.68	FC 4	0.9996	98.8 2.0	1.0164	96.9	3.750	0.3635	1.68	-1.9
2.98	494	20×21	67.20	FC 4	0.9998	92.3 4.6	1.0125	86.2	4.171	0.3597	1.25	-6.2
2.98	494	21×22	60.88	FC 165		88.9 0.6						
2.98	494	21×22	60.88	FC 4		94.6 2.8						
					Average	91.9 2.9						
4.24	704	20×20	64.40	FC 4	0.9997	74.4 1.9	1.0078	68.7	5.135	0.3526	0.81	-3.8
4.24	704	20×20	64.40	FC 165		71.1 4.0						
4.24	704	20×20	60.87	FC 165		68.7 8.0						
					Average	71.4 2.9						
5.55	922	21×21	62.36	FC 4	1.0004	61.0 1.8	1.0039	57.1	6.050	0.3453	0.35	-6.4

(1) Since the core of which water to fuel volume ratio is 1.77 was subcritical with 590 rods of fuel, experimental β_{eff}/ℓ was estimated on the critical water level extraporated by inverse multiplication method. The calculation was carried out about the core of which fuel rod array was 26×26.

(2) FC 4 and FC 165 are fission counters ;

(3) (Calculated - Measured) / Measured

(4) Temperature and ^{241}Pu decay effects are corrected to be compared with calculation.

Table 13 UO_2 lattices

Core name	1.50 U	1.83 U	2.48 U	2.96 U
Lattice pitch (cm)	1.849	1.956	2.150	2.293
Critical water level (cm)	99.20	81.28	86.89	91.60
Fuel rod array	26×26	17×17+20	15×15	15×15
Number of fuel rods at critical	361	309	225	225
Water to fuel volume ratio	1.50	1.83	2.48	2.96

Temperature of core is about 20 °C

Table 14 Measured and calculated results of β_{eff}/ℓ for UO_2 lattices

Water to fuel volume ratio	Measured		Calculated				Difference of β/ℓ %
	K_{eff}	β_{eff}/ℓ sec^{-1}	K_{eff}	β_{eff}/ℓ sec^{-1}	ℓ $\times10^{-5}$sec	β_{eff} $\times10^{-2}$	
1.50	1.0000	218.8±1.3	0.999	218.1	3.432	0.7484	-0.3
1.83	1.0000	201.3±3.3	1.000	201.4	3.714	0.7478	0.1
2.48	1.0000	174.8±3.4	0.998	167.9	4.422	0.7423	-3.9
2.96	1.0000	160.6±4.5	1.000	152.3	4.841	0.7372	-5.2

Table 15 $\frac{1}{\beta_{eff}}\cdot\frac{M^2}{K_\infty}$

Water to fuel volume ratio	H/Pu	$\frac{1}{\beta_{eff}}\cdot\frac{M^2}{K_\infty}$ (cm^2)
2.42	402	7945±250
2.98	494	7828±446
		8252 ± 72
		7948±331
4.24	704	8220±249
		8831±552
		8278±1007
5.55	922	8820±419

$$\frac{1}{\beta_{eff}}\cdot\frac{M^2}{K_\infty} = 1.74R + 7.25\times10^3, \quad R = H/Pu$$

Table 16 M^2/K_∞

Water to fuel volume ratio	H/Pu	a/a_c	β_{eff}	M^2/K_∞	Calculated M^2/K_∞	
					LASER cm^2	UGMG42 cm^2
1.77	295	7732	0.3846	29.7 1.0	34.2	35.0
2.42	402	7925	0.3635	28.8 1.0	30.4	29.6
2.98	494	8029	0.3597	29.1 1.0	28.9	28.3
4.24	704	8466	0.3526	29.9 1.0	27.6	27.3
5.55	922	8856	0.3453	30.6 1.0	27.9	27.7

Table 17 Spectrum calculation methods

	UGMG42-THERMOS	LASER
Fast section		
Number of energy groups	54 groups	50 groups
Spatial dependence	B1 applox.	B1 applox.
Slowing down model		
Hydrogen	Greuling-Goerzel	Greuling-Goerzel
Other nuclides	Consistent age applox.	Consistent age applox.
Resonance escape probability		
L-factor		
^{238}U		Strawbridge's eq.
Other nuclides		1.0
Dancoff coefficient	Fukai's model	
Resonance applox.	I.R. applox.	
Temperate	20°C	20°C
Thermal section		
Number of energy groups	30 groups	35 groups
Scattering model	Nelkin with transport correction	Nelkin with transport correction
Cell boundary condition	Isotropic scattering	Isotropic scattering
Temperature	20°C	20°C

Table 18 Source of Cross-section

Nuclide	Source	Reference
UGMG42-THERMOS library		
^{235}U, ^{238}U, ^{240}Pu, ^{241}Pu, and Zr	JNDC set	JAERI-1176 (1967)
^{239}Pu, ^{242}Pu, and H(σ_a)	ENDF/B-1	BNL 50066 (T-467) (1966)
O	UKNDL	AEEW-M802 (1967)
LASER library		
^{238}Pu	ENDF/B-2	
^{241}Am fast section	ENDF/B-2	
thermal section	GGC-4 library	GA-9021
Other nuclides	Original LASER	WCAP-6073

In UGMG42-THERMOS library, the atomic number densities of ^{238}Pu and ^{241}Am were added to that of ^{242}Pu.

Table 19 Regionwise atomic number density for spectrum calculation

X 10^{24} atom/cm^3

		May 16,1972 (330 days after)	December 22,1972 (550 days after)
Fuel	^{235}U	9.4018×10^{-5}	9.4018×10^{-5}
	^{238}U	1.2963×10^{-2}	1.2963×10^{-2}
	^{238}Pu	1.9929×10^{-6}	1.9831×10^{-6}
	^{239}Pu	2.7539×10^{-4}	2.7539×10^{-4}
	^{240}Pu	8.8585×10^{-5}	8.8585×10^{-5}
	^{241}Pu	2.8099×10^{-5}	2.7286×10^{-5}
	^{242}Pu	8.1251×10^{-6}	8.1251×10^{-6}
	^{237}Np	3.5502×10^{-9}	3.5502×10^{-9}
	^{241}Am	1.2357×10^{-6}	2.0388×10^{-6}
	O	2.7864×10^{-2}	2.7864×10^{-2}
*Cladding	Zircaloy-2	3.840×10^{-2}	3.840×10^{-2}
Moderator	H_2O	3.338×10^{-2}	3.338×10^{-2}

* Including air gap region.

Table 20 Neutron energy scheme in diffusion calculation

	UGMG42-THERMOS		LASER
Group	4 groups	3 groups	3 groups
1	10 Mev ~ 821 kev	10 Mev ~ 5.53 kev	10 Mev ~ 5.53 kev
2	821 kev ~ 5.53 kev	5.53 kev ~ 0.625 ev	5.53 kev ~ 1.855 ev
3	5.53 kev ~ 0.625 ev	0.625 ev ~ 0.0 ev	1.855 ev ~ 0.0 ev
4	0.633 ev ~ 0.0 ev		

Table 21 Three group constants calculated by LASER (May 16,1972)

Volume ratio	Group	D	Σ_a	Σ_r	Σ_f	$\nu\Sigma_f$
1.77	1	1.6765	2.4616×10^{-3}	4.4686×10^{-2}	1.0252×10^{-3}	2.9554×10^{-3}
	2	7.7426×10^{-1}	1.8954×10^{-2}	8.7907×10^{-2}	3.7062×10^{-3}	1.0425×10^{-2}
	3	2.9918×10^{-1}	1.1330×10^{-1}	0.0	6.0105×10^{-2}	1.7069×10^{-1}
2.42	1	1.6500	2.1709×10^{-3}	4.9415×10^{-2}	8.6821×10^{-4}	2.5055×10^{-3}
	2	7.3493×10^{-1}	1.6161×10^{-2}	1.0164×10^{-1}	3.1003×10^{-3}	8.7226×10^{-3}
	3	2.6498×10^{-1}	9.6800×10^{-2}	0.0	5.0631×10^{-2}	1.4367×10^{-1}
2.98	1	1.6372	1.9873×10^{-3}	5.2379×10^{-2}	7.6553×10^{-4}	2.2106×10^{-3}
	2	7.1254×10^{-1}	1.4322×10^{-2}	1.1033×10^{-1}	2.7158×10^{-3}	7.6418×10^{-3}
	3	2.4630×10^{-1}	8.6179×10^{-2}	0.0	4.4235×10^{-2}	1.2546×10^{-1}
4.24	1	1.6279	1.7044×10^{-3}	5.6989×10^{-2}	6.0243×10^{-4}	1.7418×10^{-3}
	2	6.8090×10^{-1}	1.1385×10^{-2}	1.2392×10^{-1}	2.1177×10^{-3}	5.9601×10^{-3}
	3	2.2116×10^{-1}	6.9821×10^{-2}	0.0	3.4028×10^{-2}	9.6446×10^{-2}
5.55	1	1.6337	1.5211×10^{-3}	6.0069×10^{-2}	4.9312×10^{-4}	1.4273×10^{-3}
	2	6.6180×10^{-1}	9.4066×10^{-3}	1.3303×10^{-1}	1.7228×10^{-3}	4.8494×10^{-3}
	3	2.0676×10^{-1}	5.9286×10^{-2}	0.0	2.7247×10^{-2}	7.7196×10^{-2}
H_2O	1	1.6979	7.4420×10^{-4}	7.2506×10^{-2}	0.0	0.0
	2	5.9239×10^{-1}	6.2656×10^{-4}	1.7208×10^{-1}	0.0	0.0
	3	1.6077×10^{-1}	1.8869×10^{-2}	0.0	0.0	0.0

Table 22 Three group constants calculated by UGMG42-THERMOS (May 16,1972)

Volume ratio	Group	D	Σ_a	Σ_r	Σ_f	$\nu\Sigma_f$
1.77	1	1.5950	2.2860×10^{-3}	4.5508×10^{-2}	1.0085×10^{-3}	2.8629×10^{-3}
	2	7.0563×10^{-1}	2.0879×10^{-2}	7.3676×10^{-2}	3.2211×10^{-3}	8.9280×10^{-3}
	3	3.6523×10^{-1}	1.2119×10^{-1}	0.0	6.9082×10^{-2}	1.9423×10^{-1}
2.42	1	1.5730	1.9426×10^{-3}	5.0235×10^{-2}	8.5546×10^{-4}	2.4300×10^{-3}
	2	6.8340×10^{-1}	1.8594×10^{-2}	8.5549×10^{-2}	2.7459×10^{-3}	7.6130×10^{-3}
	3	3.2032×10^{-1}	1.0171×10^{-1}	0.0	5.6199×10^{-2}	1.5788×10^{-1}
2.98	1	1.5621	1.7264×10^{-3}	5.3188×10^{-2}	7.5472×10^{-4}	2.1447×10^{-3}
	2	6.7073×10^{-1}	1.6876×10^{-2}	9.3194×10^{-2}	2.4291×10^{-3}	6.7357×10^{-3}
	3	2.9311×10^{-1}	8.9748×10^{-2}	0.0	4.8205×10^{-2}	1.3536×10^{-1}
4.24	1	1.5539	1.3940×10^{-3}	5.7765×10^{-2}	5.9446×10^{-4}	1.6905×10^{-3}
	2	6.5290×10^{-1}	1.3858×10^{-2}	1.0532×10^{-1}	1.9187×10^{-3}	5.3215×10^{-3}
	3	2.5260×10^{-1}	7.1809×10^{-2}	0.0	3.6119×10^{-2}	1.0135×10^{-1}
5.55	1	1.5578	1.1772×10^{-3}	6.0834×10^{-2}	4.8664×10^{-4}	1.3847×10^{-3}
	2	6.4205×10^{-1}	1.1671×10^{-2}	1.1359×10^{-1}	1.5720×10^{-3}	4.3602×10^{-3}
	3	2.2713×10^{-1}	6.0496×10^{-2}	0.0	2.8438×10^{-2}	7.9768×10^{-2}
H_2O	1	1.4865	2.2911×10^{-4}	7.2409×10^{-2}	0.0	0.0
	2	6.0423×10^{-1}	9.4350×10^{-4}	1.4744×10^{-1}	0.0	0.0
	3	1.3355×10^{-1}	1.9120×10^{-2}	0.0	0.0	0.0

Table 23 Four group constants calculated by UGMG42-THERMOS (May 16,1972)

Volume ratio	Group	D	Σ_a	Σ_r	Σ_f	$\nu\Sigma_f$
1.77	1	2.1184	2.8593×10^{-3}	8.1872×10^{-2}	1.9073×10^{-3}	5.4229×10^{-3}
	2	1.1468	1.7950×10^{-3}	8.4482×10^{-2}	2.3871×10^{-4}	6.7057×10^{-4}
	3	7.0563×10^{-1}	2.0879×10^{-2}	7.3676×10^{-2}	3.2211×10^{-3}	8.9280×10^{-3}
	4	3.6523×10^{-1}	1.2119×10^{-1}	0.0	6.9082×10^{-2}	1.9423×10^{-1}
2.42	1	2.0693	2.4515×10^{-3}	8.6693×10^{-2}	1.5883×10^{-3}	4.5188×10^{-3}
	2	1.1274	1.4858×10^{-3}	9.5333×10^{-2}	1.9754×10^{-4}	5.5492×10^{-4}
	3	6.8340×10^{-1}	1.8594×10^{-2}	8.5549×10^{-2}	2.7459×10^{-3}	7.6130×10^{-3}
	4	3.2032×10^{-1}	1.0171×10^{-1}	0.0	5.6199×10^{-2}	1.5788×10^{-1}
2.98	1	2.0460	2.1965×10^{-3}	8.9663×10^{-2}	1.3877×10^{-3}	3.9496×10^{-3}
	2	1.1167	1.2937×10^{-3}	1.0216×10^{-1}	1.7195×10^{-4}	4.8301×10^{-4}
	3	6.7073×10^{-1}	1.6876×10^{-2}	9.3194×10^{-2}	2.4291×10^{-3}	6.7357×10^{-3}
	4	2.9311×10^{-1}	8.9748×10^{-2}	0.0	4.8205×10^{-2}	1.3536×10^{-1}
4.24	1	2.0274	1.8069×10^{-3}	9.4085×10^{-2}	1.0791×10^{-3}	3.0736×10^{-3}
	2	1.1029	1.0010×10^{-3}	1.1277×10^{-1}	1.3293×10^{-4}	3.7339×10^{-4}
	3	6.5290×10^{-1}	1.3858×10^{-2}	1.0532×10^{-1}	1.9187×10^{-3}	5.3215×10^{-3}
	4	2.5260×10^{-1}	7.1809×10^{-2}	0.0	3.6119×10^{-2}	1.0135×10^{-1}
5.55	1	2.0331	1.5546×10^{-3}	9.6826×10^{-2}	8.7702×10^{-4}	2.4995×10^{-3}
	2	1.0963	8.1063×10^{-4}	1.1991×10^{-1}	1.0755×10^{-4}	3.0210×10^{-4}
	3	6.4205×10^{-1}	1.1671×10^{-2}	1.1359×10^{-1}	1.5720×10^{-3}	4.3602×10^{-3}
	4	2.2713×10^{-1}	6.0496×10^{-2}	0.0	2.8438×10^{-2}	7.9768×10^{-2}
H_2O	1	1.9009	4.4829×10^{-4}	1.0961×10^{-1}	0.0	0.0
	2	1.0534	0.0	1.4810×10^{-1}	0.0	0.0
	3	6.0423×10^{-1}	9.4350×10^{-4}	1.4744×10^{-1}	0.0	0.0
	4	1.3355×10^{-1}	1.9120×10^{-2}	0.0	0.0	0.0

Table 24 Corrected multiplication factor to be compared with calculational results

Water to fuel volume ratio	^{241}Pu decay and temperature correction							Correction to the vertical reflector saving 12.0 cm in the calculation		Measured K_{eff} to be compared with the calculational results
	Date & Run Number	Days to May 16, 1972	$\Delta\rho$ by ^{241}Pu decay cent	Temp. °C	$\Delta\rho$ by Temperature difference cent	Total reactivity effect		Reactivity effect due to λ_z		
						cent	%ΔK/K	cent	%ΔK/K	
1.77	Sep.27,'72 5220	+134	+38.9	21.3	+2.1	+41.0	+0.158	-53.1	-0.193	0.9940 ± 0.0007
2.42	June 6,'72 5103	+ 21	+ 6.1	18.7	+1.0	+ 7.1	+0.025	-14.4	-0.052	0.9997 ± 0.0001
2.98	May 18,'72 5094	+ 3	+ 0.9	17.6	+0.4	+ 1.3	+0.005	----	-----	1.0001 ± 0.0001
4.24	Apr.13,'72 5060	- 32	- 8.6	13.2	-8.8	-17.4	-0.061	+17.6	+0.062	1.0000 ± 0.0001
5.55	Apr.28,'72 5080	- 17	- 4.4	18.0	-6.9	-11.3	-0.039	+30.3	+0.105	1.0007 ± 0.0001

Calculation is carried out at 20°C and using the atomic number densities of 330 days after the plutonium purification.

Table 25 Calculational results of K_{eff}

Warer to fuel volume ratio	H/Pu	Fuel rod array	Lattice pitch (cm)	Critical water level (cm)	K_{eff}			Difference from experiment	
					Experiment	Calculation by PDQ-5		LASER (%δK/K)	UGMG42-TH (%δK/K)
						LASER	UGMG42-TH.		
1.77	295	*	1.660	68.79	0.9940	0.9916	1.0153	-0.24	2.14
2.42	402	22x22	1.825	69.38	0.9997	1.0013	1.0145	0.16	1.46
2.98	494	21x21	1.956	61.49	1.0001	1.0033	1.0110	0.32	1.08
4.24	704	20x20	2.225	60.56	1.0000	1.0066	1.0070	0.65	0.69
5.55	922	21x21	2.474	62.21	1.0007	1.0077	1.0035	0.70	0.28

* Cylindrical core with 640 rods

Table 26 Calculated Thermal Neutron Speed and Depression Factor

V.R.	Average thermal neutron velocity, $\overline{v}_b$ (x2200 m/sec)		Thermal neutron flux depression factor, $d = \phi_b/\phi_{av}$	
	LASER	UGMG42-THERMOS	LASER	UGMG42-THERMOS
1.77	1.551	1.370	1.09	1.11
2.42	1.447	1.313	1.09	1.10
2.98	1.393	1.283	1.08	1.10
4.24	1.323	1.243	1.08	1.09
5.55	1.285	1.221	1.08	1.09
H_2O*	1.175	1.158	1.00	1.00

*These data are used in the reflector region.

Table 27 R_{cd}^{-1} and $\Sigma_{r,2}/\Sigma_{a,3}$

Water to fuel volume ratio	H/Pu	R_{cd}^{-1}	$\Sigma_{r,2}/\Sigma_{a,3}$	
			LASER	UGMG42-THERMOS
1.77	295		0.7759	0.6079
2.42	402	2.25 ± 0.09	1.0500	0.8411
2.98	494	2.78 ± 0.07	1.2802	1.0384
4.24	704	3.80 ± 0.13	1.7748	1.4667
5.55	922	5.10 ± 0.13	2.2439	1.8776

Table 28 Root Mean Square Difference of Calculated Power to Experimented

Water to fuel volume ratio	LASER-PDQ5		UGMG42-THERMOS-PDQ5	
	X-Y direction	Diagonal direction	X-Y direction	Diagonal direction
1.77				
2.42	1.2	1.7	1.8	3.3
2.98	1.2	2.0	1.8	3.4
4.24	1.3	2.9	2.2	4.9
5.55	1.6	1.9	2.2	3.7

Table 29 Change of Pu Compositions

wt %

	May 16, 1972 330 days after purification	December 22, 1972 550 days after purification
^{238}Pu	0.491	0.488
^{239}Pu	68.1	68.1
^{240}Pu	22.0	22.0
^{241}Pu	7.01	6.81
^{242}Pu	2.03	2.03
^{241}Am	0.308	0.506

Table 30 Three group constants calculated by LASER (December 22,1972)

Volume ratio	Group	D	Σ_a	Σ_r	Σ_f	$\nu\Sigma_f$
1.77	1	1.6770	2.4609×10^{-3}	4.4691×10^{-2}	1.0243×10^{-3}	2.9527×10^{-3}
	2	7.7429×10^{-1}	1.8942×10^{-2}	8.7940×10^{-2}	3.6893×10^{-3}	1.0374×10^{-2}
	3	2.9909×10^{-1}	1.1322×10^{-1}	0.0	5.9943×10^{-2}	1.7021×10^{-1}
2.42	1	1.6504	2.1703×10^{-3}	4.9420×10^{-2}	8.6748×10^{-4}	2.5032×10^{-3}
	2	7.3496×10^{-1}	1.6151×10^{-2}	1.0167×10^{-1}	3.0862×10^{-3}	8.6803×10^{-3}
	3	2.6492×10^{-1}	9.6723×10^{-2}	0.0	5.0491×10^{-2}	1.4326×10^{-1}
2.98	1	1.6377	1.9868×10^{-3}	5.2384×10^{-2}	7.6489×10^{-4}	2.2087×10^{-3}
	2	7.1256×10^{-1}	1.4313×10^{-2}	1.1036×10^{-1}	2.7033×10^{-3}	7.6046×10^{-3}
	3	2.4625×10^{-1}	8.6106×10^{-2}	0.0	4.4112×10^{-2}	1.2510×10^{-2}
4.24	1	1.6284	1.7040×10^{-3}	5.6995×10^{-2}	6.0194×10^{-4}	1.7403×10^{-3}
	2	6.8092×10^{-1}	1.1377×10^{-3}	1.2394×10^{-1}	2.1080×10^{-3}	5.9311×10^{-3}
	3	2.2112×10^{-1}	6.9760×10^{-2}	0.0	3.3932×10^{-2}	9.6166×10^{-2}
5.55	1	1.6343	1.5209×10^{-3}	6.0074×10^{-2}	4.9273×10^{-4}	1.4261×10^{-3}
	2	6.6181×10^{-1}	9.4002×10^{-3}	1.3305×10^{-1}	1.7149×10^{-3}	4.8258×10^{-3}
	3	2.0673×10^{-1}	5.9235×10^{-2}	0.0	2.7170×10^{-2}	7.6971×10^{-2}

Table 31 Calculated Reactivity Effect due to ^{241}Pu Decay to ^{241}Am

Water to fuel volume ratio	K_{eff}		$-\Delta K$	β_{eff} %	$-\rho$ cent	$d\rho/dt$ cent/day	
	May 16, '72	December 22, '72				Calculation	Experiment
2.42	1.0013	0.9992	0.0021	0.3635	57	0.26	0.28 ± 0.02
2.98	1.0033	1.0012	0.0021	0.3597	57	0.26	0.29 ± 0.02
4.24	1.0066	1.0045	0.0021	0.3526	59	0.27	0.27 ± 0.02
5.55	1.0077	1.0056	0.0021	0.3453	61	0.28	0.26 ± 0.02

Table 32 Calculated Horizontal Reflector Savings

Water to fuel volume ratio	Horizontal reflector saving, λ_H, cm		
	LASER	UGMG42-THERMOS	Experiment
1.77	15.9	17.0	15.7 ± 0.3
2.42	14.7	15.7	14.6 ± 0.3
2.98	14.0	15.0	14.1 ± 0.3
4.24	13.2	14.1	13.4 ± 0.2
5.55	12.8	13.5	13.1 ± 0.2

Table 33 Delayed Neutron Parameters

Group / Water to fuel volume ratio i	Effective delayed neutron fraction, β_i						β_{eff}
	1	2	3	4	5	6	
2.42	0.0279	0.247	0.197	0.357	0.127	0.0437	0.00364
2.98	0.0282	0.249	0.198	0.357	0.125	0.0431	0.00360
4.24	0.0285	0.252	0.198	0.357	0.122	0.0422	0.00350
5.55	0.0287	0.253	0.199	0.357	0.121	0.0416	0.00345
	Decay constant, λ_i (sec)						
	0.0124	0.0305	0.111	0.301	1.13	3.00	

Appendix 1. Digital values of Au activity distributons.

TABLE 1 SUB-CD AND EPI-CD ACTIVATION TRAVERSE BY AU-WIRE
(V.R.=1.77 , RUN NO.=5237)

NO.	*SUB-CD* DISTANCE	*SUB-CD* ACTIVITY	*EPI-CD* DISTANCE	*EPI-CD* ACTIVITY
1	0.34	1.216	0.03	1.259
2	0.47	1.201	0.80	1.251
3	1.14	1.153	0.85	1.252
4	1.30	1.237	1.64	1.235
5	1.96	1.250	1.68	1.234
6	2.15	1.204	2.48	1.218
7	2.79	1.133	2.50	1.262
8	2.99	1.196	3.30	1.266
9	3.63	1.171	3.30	1.220
10	3.80	1.158	4.13	1.216
11	4.47	1.150	4.14	1.224
12	4.63	1.157	4.95	1.205
13	5.30	1.172	4.97	1.208
14	5.46	1.170	5.79	1.183
15	6.14	1.113	5.81	1.184
16	6.29	1.162	6.63	1.185
17	6.98	1.141	6.64	1.226
18	7.14	1.121	7.46	1.134
19	7.81	1.115	7.46	1.136
20	7.98	1.121	8.29	1.156
21	8.64	1.066	8.31	1.131
22	8.83	1.073	9.13	1.083
23	9.45	1.038	9.16	1.093
24	9.66	1.007	9.96	1.089
25	10.28	1.012	9.98	1.103
26	10.47	1.008	10.79	1.038
27	11.11	1.006	10.82	1.036
28	11.32	1.008	11.62	1.033
29	11.94	0.975	11.67	1.025
30	12.15	0.933	12.44	0.964
31	12.77	0.890	12.49	0.966
32	12.97	0.940	13.26	0.953
33	13.60	0.888	13.31	0.927
34	13.79	0.880	14.10	0.902
35	14.43	0.831	14.15	0.916
36	14.63	0.845	14.94	0.875
37	15.26	0.805	15.01	0.869
38	15.45	0.814	15.77	0.833
39	16.10	0.749	15.84	0.820
40	16.28	0.837	16.61	0.814
41	16.92	0.750	16.67	0.784
42	17.12	0.719	17.43	0.759
43	17.73	0.733	17.52	0.745
44	17.95	0.747	18.24	0.713
45	18.57	0.729	18.32	0.700
46	18.77	0.723	19.07	0.640
47	19.41	0.816	19.11	0.639
48	19.61	0.804	19.91	0.604
49	20.24	0.896	19.94	0.603
50	20.44	0.898	20.73	0.552

Table 1 continued.

NO.	*SUB-CD* Distance	*SUB-CD* Activity	*EPI-CD* Distance	*EPI-CD* Activity
51	20.87	1.003	20.77	0.539
52	21.26	1.220	21.59	0.532
53	21.32	1.018	21.64	0.524
54	21.82	1.728	22.56	0.462
55	21.88	1.745	22.60	0.454
56	22.33	2.069	23.55	0.394
57	22.34	2.033	23.62	0.386
58	22.82	2.310	24.54	0.328
59	22.86	2.290	24.64	0.331
60	23.31	2.489	25.53	0.256
61	23.35	2.449	25.62	0.268
62	23.84	2.497	26.51	0.212
63	24.05	2.433	27.51	0.168
64	24.34	2.549	28.50	0.138
65	25.05	2.427	29.49	0.105
66	25.09	2.375	30.49	0.079
67	26.05	2.213	31.48	0.069
68	26.08	2.311	0.00	0.000
69	27.03	2.028	0.00	0.000
70	28.01	1.733	0.00	0.000
71	29.00	1.519	0.00	0.000
72	30.00	1.284	0.00	0.000
73	31.00	1.042	0.00	0.000

TABLE 2 SUB-CD AND EPI-CD ACTIVATION TRAVERSE BY AU-WIRE
(V.R.=2.42 , RUN NO.=5113)

NO.	*SUB-CD* DISTANCE	*SUB-CD* ACTIVITY	*EPI-CD* DISTANCE	*EPI-CD* ACTIVITY
1	0.37	1.235	0.37	1.238
2	0.54	1.178	0.54	1.265
3	1.29	1.127	1.29	1.246
4	1.43	1.230	1.43	1.241
5	2.19	1.160	2.19	1.225
6	2.35	1.184	2.35	1.252
7	3.10	1.115	3.10	1.231
8	3.26	1.227	3.26	1.248
9	4.00	1.142	4.00	1.254
10	4.17	1.157	4.17	1.232
11	4.91	1.116	4.91	1.193
12	5.07	1.207	5.07	1.216
13	5.81	1.115	5.81	1.200
14	5.96	1.140	5.96	1.188
15	6.71	1.028	6.71	1.174
16	6.89	1.106	6.89	1.173
17	7.63	1.076	7.63	1.154
18	7.81	1.088	7.81	1.138
19	8.55	1.027	8.55	1.126
20	8.72	1.092	8.72	1.100
21	9.46	1.058	9.46	1.080
22	9.63	1.012	9.63	1.057
23	10.37	1.000	10.37	1.039
24	10.54	0.982	10.54	1.048
25	11.28	1.023	11.28	1.005
26	11.45	0.981	11.45	1.004
27	12.19	0.914	12.19	0.978
28	12.36	0.933	12.36	0.952
29	13.10	0.856	13.10	0.917
30	13.27	0.886	13.27	0.924
31	14.00	0.752	14.00	0.868
32	14.18	0.846	14.18	0.876
33	14.90	0.801	14.90	0.826
34	15.09	0.788	15.09	0.829
35	15.81	0.786	15.81	0.760
36	16.00	0.770	16.00	0.748
37	16.72	0.767	16.72	0.718
38	16.92	0.764	16.92	0.691
39	17.63	0.742	17.63	0.661
40	17.83	0.790	17.83	0.649
41	18.56	0.856	18.56	0.599
42	18.75	0.845	18.75	0.586
43	19.54	1.014	19.54	0.542
44	19.67	1.085	19.67	0.547
45	20.52	1.510	20.52	0.498
46	20.59	1.522	20.59	0.491
47	21.52	1.821	21.52	0.433
48	22.51	1.875	22.51	0.354
49	23.52	1.840	23.52	0.285

TABLE 3 SUB-CD AND EPI-CD ACTIVATION TRAVERSE BY AU-WIRE
(V.R.=2.98 , RUN NO.=5099)

NO.	*SUB-CD* DISTANCE	*SUB-CD* ACTIVITY	*EPI-CD* DISTANCE	*EPI-CD* ACTIVITY
1	0.25	1.191	0.25	1.267
2	0.73	1.224	0.73	1.275
3	1.22	1.237	1.22	1.263
4	1.71	1.275	1.71	1.254
5	2.19	1.182	2.19	1.280
6	2.68	1.183	2.68	1.263
7	3.19	1.201	3.19	1.245
8	3.66	1.204	3.66	1.220
9	4.16	1.168	4.16	1.252
10	4.63	1.180	4.63	1.225
11	5.14	1.183	5.14	1.210
12	5.61	1.154	5.61	1.216
13	6.12	1.124	6.12	1.216
14	6.59	1.149	6.59	1.193
15	7.09	1.110	7.09	1.191
16	7.56	1.120	7.56	1.143
17	8.07	1.072	8.07	1.144
18	8.54	1.101	8.54	1.138
19	9.04	1.052	9.04	1.084
20	9.52	1.039	9.52	1.073
21	10.02	1.019	10.02	1.058
22	10.49	1.040	10.49	1.032
23	11.00	0.978	11.00	1.011
24	11.47	0.964	11.47	1.021
25	11.98	0.938	11.98	0.975
26	12.45	0.938	12.45	1.000
27	12.96	0.916	12.96	0.956
28	13.43	0.884	13.43	0.941
29	13.95	0.841	13.95	0.862
30	14.40	0.849	14.40	0.859
31	14.92	0.800	14.92	0.848
32	15.37	0.820	15.37	0.810
33	15.90	0.756	15.90	0.777
34	16.35	0.767	16.35	0.776
35	16.88	0.745	16.88	0.714
36	17.32	0.757	17.32	0.697
37	17.85	0.715	17.85	0.678
38	18.31	0.747	18.31	0.630
39	18.84	0.771	18.84	0.599
40	19.30	0.793	19.30	0.550
41	19.82	0.872	19.82	0.531
42	20.29	0.943	20.29	0.521
43	20.80	1.237	20.80	0.486
44	21.32	1.292	21.32	0.446
45	21.76	1.433	21.76	0.408
46	22.74	1.481	22.74	0.344
47	23.73	1.430	23.73	0.268

TABLE 4 SUB-CD AND EPI-CD ACTIVATION TRAVERSE BY AU-WIRE
(V.R.=4.24 , RUN NO.=5069)

NO.	*SUB-CD* DISTANCE	*SUB-CD* ACTIVITY	*EPI-CD* DISTANCE	*EPI-CD* ACTIVITY
1	0.01	1.280	0.01	1.260
2	1.12	1.191	1.12	1.297
3	1.12	1.219	1.12	1.247
4	2.22	1.264	2.22	1.278
5	2.23	1.261	2.23	1.265
6	3.33	1.225	3.33	1.255
7	3.35	1.216	3.35	1.240
8	4.44	1.259	4.44	1.259
9	4.47	1.265	4.47	1.226
10	5.54	1.202	5.54	1.240
11	5.58	1.154	5.58	1.184
12	6.66	1.203	6.66	1.217
13	6.69	1.176	6.69	1.221
14	7.78	1.136	7.78	1.160
15	7.81	1.082	7.81	1.169
16	8.91	1.156	8.91	1.111
17	8.93	1.148	8.93	1.138
18	10.02	1.040	10.02	1.125
19	10.06	1.061	10.06	1.065
20	11.10	1.066	11.10	1.045
21	11.20	1.019	11.20	1.056
22	12.25	0.969	12.25	1.007
23	12.34	0.964	12.34	1.000
24	13.38	0.949	13.38	0.976
25	13.44	0.902	13.44	0.952
26	14.47	0.848	14.47	0.920
27	14.52	0.879	14.52	0.883
28	15.57	0.876	15.57	0.853
29	15.60	0.852	15.60	0.828
30	16.68	0.789	16.68	0.809
31	16.72	0.778	16.72	0.771
32	17.80	0.745	17.80	0.734
33	17.86	0.752	17.86	0.718
34	18.91	0.662	18.91	0.662
35	19.00	0.647	19.00	0.628
36	20.03	0.694	20.03	0.597
37	20.10	0.684	20.10	0.582
38	21.13	0.692	21.13	0.526
39	21.18	0.692	21.18	0.497
40	22.21	0.826	22.21	0.477
41	22.26	0.901	22.26	0.441
42	23.24	1.004	23.24	0.403
43	23.27	1.016	23.27	0.387
44	24.24	1.023	24.24	0.340
45	24.27	1.048	24.27	0.321
46	25.26	1.011	25.26	0.277
47	25.27	1.000	25.27	0.268

TABLE 5 SUB-CD AND EPI-CD ACTIVATION TRAVERSE BY AU-WIRE
(V.R.=5.55 , RUN NO.=5237)

NO.	*SUB-CD* DISTANCE	*SUB-CD* ACTIVITY	*EPI-CD* DISTANCE	*EPI-CD* ACTIVITY
1	0.11	1.260	0.11	1.271
2	1.11	1.314	1.11	1.288
3	1.35	1.313	1.35	1.278
4	2.35	1.252	2.35	1.295
5	2.56	1.241	2.56	1.290
6	3.61	1.293	3.61	1.300
7	3.77	1.295	3.77	1.295
8	4.86	1.229	4.86	1.246
9	5.00	1.218	5.00	1.262
10	6.11	1.246	6.11	1.259
11	6.24	1.244	6.24	1.237
12	7.34	1.178	7.34	1.215
13	7.47	1.164	7.47	1.201
14	8.58	1.214	8.58	1.208
15	8.71	1.188	8.71	1.202
16	9.86	1.118	9.86	1.163
17	9.93	1.107	9.93	1.148
18	11.13	1.140	11.13	1.111
19	11.13	1.116	11.13	1.145
20	12.32	1.060	12.32	1.065
21	12.38	1.066	12.38	1.085
22	13.55	1.050	13.55	1.039
23	13.63	1.046	13.63	1.036
24	14.79	0.963	14.79	0.981
25	14.88	0.948	14.88	0.993
26	16.02	0.960	16.02	0.926
27	16.11	0.941	16.11	0.933
28	17.25	0.853	17.25	0.867
29	17.35	0.843	17.35	0.884
30	18.49	0.832	18.49	0.822
31	18.58	0.810	18.58	0.830
32	19.70	0.754	19.70	0.740
33	19.79	0.717	19.79	0.762
34	20.92	0.700	20.92	0.678
35	21.02	0.684	21.02	0.694
36	22.14	0.633	22.14	0.598
37	22.25	0.612	22.25	0.620
38	23.41	0.621	23.41	0.556
39	23.49	0.598	23.49	0.554
40	24.67	0.589	24.67	0.456
41	24.73	0.591	24.73	0.465
42	25.80	0.678	25.80	0.398
43	25.85	0.695	25.85	0.405
44	26.83	0.752	26.83	0.337
45	26.85	0.765	26.85	0.352
46	27.83	0.780	27.83	0.273
47	27.84	0.754	27.84	0.290
48	28.82	0.757	28.82	0.231
49	28.83	0.713	28.83	0.246
50	29.81	0.689	29.81	0.189
51	29.82	0.671	29.82	0.101

TABLE 6 CD-RATIO=1.0 (V.R.=1.77, RUN NO.=5237)

NO.	DISTANCE	CD-RATIO-1	NO.	DISTANCE	CD-RATIO - 1
1	0.34	1.740	51	20.87	3.150
2	0.47	1.710	52	21.26	4.070
3	1.14	1.650	53	21.32	3.380
4	1.30	1.770	54	21.82	6.000
5	1.96	1.800	55	21.88	6.290
6	2.15	1.730	56	22.33	7.760
7	2.79	1.640	57	22.34	7.790
8	2.99	1.730	58	22.82	9.220
9	3.63	1.710	59	22.86	9.390
10	3.80	1.690	60	23.31	10.680
11	4.47	1.700	61	23.35	10.730
12	4.63	1.710	62	23.84	11.870
13	5.30	1.750	63	24.05	11.540
14	5.46	1.750			
15	6.14	1.690			
16	6.29	1.760			
17	6.98	1.760			
18	7.14	1.730			
19	7.81	1.750			
20	7.98	1.760			
21	8.64	1.710			
22	8.83	1.720			
23	9.45	1.700			
24	9.66	1.650			
25	10.28	1.690			
26	10.47	1.700			
27	11.11	1.730			
28	11.32	1.750			
29	11.94	1.730			
30	12.15	1.680			
31	12.77	1.630			
32	12.97	1.750			
33	13.60	1.680			
34	13.79	1.700			
35	14.43	1.650			
36	14.63	1.700			
37	15.26	1.660			
38	15.45	1.720			
39	16.10	1.630			
40	16.28	1.840			
41	16.92	1.730			
42	17.12	1.700			
43	17.73	1.770			
44	17.95	1.860			
45	18.57	1.870			
46	18.77	1.910			
47	19.41	2.260			
48	19.61	2.300			
49	20.24	2.660			
50	20.44	2.740			

TABLE 7 CD-RATIO-1.0 (V.R.=2.42, RUN NO.=5113)

NO.	DISTANCE	CD-RATIO-1
1	0.37	2.360
2	0.54	2.210
3	1.29	2.140
4	1.43	2.350
5	2.19	2.240
6	2.35	2.240
7	3.10	2.150
8	3.26	2.330
9	4.00	2.160
10	4.17	2.230
11	4.91	2.220
12	5.07	2.350
13	5.81	2.200
14	5.96	2.270
15	6.71	2.080
16	6.89	2.230
17	7.63	2.210
18	7.81	2.270
19	8.55	2.160
20	8.72	2.350
21	9.46	2.320
22	9.63	2.270
23	10.37	2.280
24	10.54	2.220
25	11.28	2.410
26	11.45	2.310
27	12.19	2.220
28	12.36	2.320
29	13.10	2.210
30	13.27	2.270
31	14.00	2.050
32	14.18	2.290
33	14.90	2.300
34	15.09	2.250
35	15.81	2.450
36	16.00	2.440
37	16.72	2.530
38	16.92	2.620
39	17.63	2.660
40	17.83	2.880
41	18.56	3.390
42	18.75	3.420
43	19.54	4.430
44	19.67	4.700
45	20.52	7.200
46	20.59	7.350
47	21.52	9.960

TABLE 8 CD-RATIO-1.0 (V.R.=2.98, RUN NO.=5099)

NO.	DISTANCE	CD-RATIO-1
1	0.25	2.720
2	0.73	2.780
3	1.22	2.830
4	1.71	2.940
5	2.19	2.790
6	2.68	2.710
7	3.19	2.790
8	3.66	2.850
9	4.16	2.700
10	4.63	2.790
11	5.14	2.830
12	5.61	2.740
13	6.12	2.670
14	6.59	2.790
15	7.09	2.700
16	7.56	2.830
17	8.07	2.710
18	8.54	2.800
19	9.04	2.810
20	9.52	2.800
21	10.02	2.790
22	10.49	2.910
23	11.00	2.800
24	11.47	2.730
25	11.98	2.780
26	12.45	2.710
27	12.96	2.770
28	13.43	2.720
29	13.95	2.820
30	14.40	2.860
31	14.92	2.730
32	15.37	2.930
33	15.90	2.810
34	16.35	2.860
35	16.88	3.020
36	17.32	3.140
37	17.85	3.050
38	18.31	3.430
39	18.84	3.720
40	19.30	4.170
41	19.82	4.750
42	20.29	5.240
43	20.80	7.370
44	21.32	8.380
45	21.76	10.150

TABLE 9 CD-RATIO-1.0 (V.R.=4.24, RUN NO.=5069)

NO.	DISTANCE	CD-RATIO-1
1	0.01	3.921
2	1.12	3.544
3	1.12	3.773
4	2.22	3.817
5	2.23	3.847
6	3.33	3.766
7	3.35	3.784
8	4.44	3.859
9	4.47	3.982
10	5.54	3.741
11	5.58	3.760
12	6.66	3.815
13	6.69	3.716
14	7.78	3.779
15	7.81	3.572
16	8.91	4.016
17	8.93	3.893
18	10.02	3.565
19	10.06	3.845
20	11.10	3.938
21	11.20	3.725
22	12.25	3.714
23	12.34	3.718
24	13.38	3.754
25	13.44	3.655
26	14.47	3.558
27	14.52	3.842
28	15.57	3.961
29	15.60	3.970
30	16.68	3.763
31	16.72	3.897
32	17.80	3.918
33	17.86	4.042
34	18.91	3.859
35	19.00	3.975
36	20.03	4.486
37	20.10	4.535
38	21.13	5.078
39	21.18	5.374
40	22.21	6.686
41	22.26	7.880
42	23.24	9.616
43	23.27	10.137

TABLE 10 CD-RATIO-1.0 (V.R.=5.55, RUN NO.=5237)

NO.	DISTANCE	CD-RATIO-1
1	0.11	5.001
2	1.11	5.147
3	1.35	5.181
4	2.35	4.876
5	2.56	4.851
6	3.61	5.016
7	3.77	5.044
8	4.86	4.976
9	5.00	4.866
10	6.11	4.991
11	6.24	5.073
12	7.34	4.889
13	7.47	4.888
14	8.58	5.069
15	8.71	4.983
16	9.86	4.846
17	9.93	4.865
18	11.13	5.174
19	11.13	4.917
20	12.32	5.021
21	12.38	4.954
22	13.55	5.096
23	13.63	5.090
24	14.79	4.951
25	14.88	4.812
26	16.02	5.226
27	16.11	5.089
28	17.25	4.960
29	17.35	4.811
30	18.49	5.102
31	18.58	4.920
32	19.70	5.142
33	19.79	4.742
34	20.92	5.204
35	21.02	4.974
36	22.14	5.337
37	22.25	4.975
38	23.41	5.631
39	23.49	5.447
40	24.67	6.515
41	24.73	6.408
42	25.80	8.597
43	25.85	8.655

Appendix 2. Digital values of power distributions.

TABLE 1 POWER DISTRIBUTION (V.R.=1.77 , RUN NO.=5225)

NO.	*HORIZONTAL* DISTANCE	REL. POWER
1	0.83	1.220
2	0.83	1.210
3	2.49	1.166
4	2.49	1.214
5	4.15	1.157
6	4.15	1.167
7	5.81	1.150
8	5.81	1.118
9	7.47	1.104
10	7.47	1.133
11	9.13	1.053
12	9.13	1.065
13	10.79	1.022
14	10.79	1.009
15	12.45	0.943
16	12.45	0.931
17	14.11	0.878
18	14.11	0.865
19	15.77	0.807
20	15.77	0.808
21	17.43	0.742
22	17.43	0.768
23	19.09	0.761
24	19.09	0.773
25	20.75	0.950
26	20.75	0.986

TABLE 2 POWER DISTRIBUTION (V.R.=2.42 , RUN NO.=5113)

NO.	*HORIZONTAL* DISTANCE	REL. POWER	*DIAGONAL* DISTANCE	REL. POWER
1	0.91	1.204	1.29	1.206
2	0.91	1.201	1.29	1.204
3	2.74	1.201	3.87	1.177
4	2.74	1.176	3.87	1.189
5	4.56	1.165	6.45	1.165
6	4.56	1.154	6.45	1.119
7	6.39	1.115	9.03	1.048
8	6.39	1.131	9.03	1.069
9	8.21	1.084	11.61	0.949
10	8.21	1.068	11.61	0.968
11	10.04	1.025	14.20	0.861
12	10.04	1.021	14.20	0.837
13	11.86	0.945	16.78	0.731
14	11.86	0.933	16.78	0.728
15	13.69	0.859	19.36	0.618
16	13.69	0.873	19.36	0.610
17	15.51	0.787	21.94	0.512
18	15.51	0.779	21.94	0.515
19	17.34	0.757	24.52	0.457
20	17.34	0.739	24.52	0.463
21	19.16	0.888	27.10	0.560
22	19.16	0.894	27.10	0.575

TABLE 3 POWER DISTRIBUTION (V.R.=2.98 , RUN NO.=5098)

NO.	*HORIZONTAL* DISTANCE	REL. POWER	*DIAGONAL* DISTANCE	REL. POWER
1	0.00	1.225	0.00	1.258
2	0.00	1.225	0.00	1.258
3	1.96	1.224	2.77	1.213
4	1.96	1.219	2.77	1.208
5	3.91	1.192	5.53	1.173
6	3.91	1.187	5.53	1.160
7	5.87	1.156	8.30	1.101
8	5.87	1.149	8.30	1.100
9	7.82	1.118	11.06	0.978
10	7.82	1.123	11.06	1.018
11	9.78	1.035	13.83	0.887
12	9.78	1.058	13.83	0.880
13	11.74	0.938	16.60	0.723
14	11.74	0.951	16.60	0.751
15	13.69	0.868	19.36	0.618
16	13.69	0.889	19.36	0.607
17	15.65	0.793	22.13	0.505
18	15.65	0.791	22.13	0.517
19	17.60	0.747	24.90	0.426
20	17.60	0.729	24.90	0.439
21	19.56	0.789	27.66	0.487
22	19.56	0.820	27.66	0.488

TABLE 4 POWER DISTRIBUTION (V.R.=4.24 , RUN NO.=5065)

NO.	*HORIZONTAL* DISTANCE	REL. POWER	*DIAGONAL* DISTANCE	REL. POWER
1	1.11	1.282	1.57	1.252
2	1.11	1.270	1.57	1.259
3	3.34	1.228	4.72	1.260
4	3.34	1.256	4.72	1.228
5	5.56	1.191	7.87	1.157
6	5.56	1.206	7.87	1.160
7	7.79	1.161	11.01	1.055
8	7.79	1.156	11.01	1.069
9	10.01	1.050	14.16	0.941
10	10.01	1.091	14.16	0.916
11	12.24	0.996	17.31	0.775
12	12.24	0.990	17.31	0.765
13	14.46	0.895	20.45	0.634
14	14.46	0.888	20.45	0.639
15	16.69	0.796	23.60	0.477
16	16.69	0.774	23.60	0.492
17	18.91	0.695	26.75	0.354
18	18.91	0.681	26.75	0.381
19	21.14	0.696	29.89	0.353
20	21.14	0.697	29.89	0.360

TABLE 5 POWER DISTRIBUTION (V.R.=5.55 , RUN NO.=5083)

NO.	*HORIZONTAL* DISTANCE	REL. POWER	*DIAGONAL* DISTANCE	REL. POWER
1	0.00	1.308	0.00	1.323
2	0.00	1.308	0.00	1.323
3	2.47	1.282	3.50	1.282
4	2.47	1.287	3.50	1.289
5	4.95	1.264	7.00	1.235
6	4.95	1.260	7.00	1.239
7	7.42	1.211	10.50	1.143
8	7.42	1.213	10.50	1.150
9	9.90	1.167	13.99	1.042
10	9.90	1.156	13.99	1.046
11	12.37	1.100	17.49	0.891
12	12.37	1.051	17.49	0.908
13	14.84	0.989	20.99	0.742
14	14.84	0.961	20.99	0.738
15	17.32	0.894	24.49	0.572
16	17.32	0.870	24.49	0.584
17	19.79	0.764	27.99	0.432
18	19.79	0.744	27.99	0.437
19	22.27	0.657	31.49	0.313
20	22.27	0.628	31.49	0.316
21	24.74	0.602	34.99	0.264
22	24.74	0.585	34.99	0.258